The Whakamaru Magmatic System (Taupō Volcanic Zone, New Zealand), Part 1: Evidence from tephra deposits for the eruption of multiple magma types through time

Harmon, Lydia J, *ljharmo1@asu.edu, ORCID 0000-0002-9985-705X, Department of Earth & Environmental Sciences, Vanderbilt University, 2301 Vanderbilt Place, Nashville, TN 37235, USA and School of Earth and Space Exploration, Arizona State University, 781 Terrace Mall, Tempe, AZ 85287, USA

Gualda, Guilherme A R, Department of Earth & Environmental Sciences, Vanderbilt University, 2301 Vanderbilt Place, Nashville, TN 37235, USA.

Gravley, Darren M, School of Earth and Environment, University of Canterbury, Private Bag 4800, Christchurch 8140, New Zealand.

Smithies, Sarah L, School of Earth and Environment, University of Canterbury, Private Bag 4800, Christchurch 8140, New Zealand.

Deering, Chad D, Michigan Tech University, Geological and Mining Engineering and Sciences, 1400 Townsend Drive, Houghton, MI 49931, USA.

ABSTRACT

The Whakamaru group eruptions (349 ± 4 ka; Downs *et al.*, 2014) are the largest known eruptions in the history of the young Taupō Volcanic Zone, Aotearoa New Zealand. The complex field relationships of the ignimbrites have thus far obscured the timing and history of their eruption(s). We present new evidence from fall deposits correlated with the Whakamaru eruptions to complement the ignimbrite record. Two coastal sections are characterized in detail. We group the tephra horizons into three packages: the older, smaller Tablelands and Paerata tephras; the overlying Kohioawa tephra (correlated with Whakamaru group eruptions); and the younger Murupara and Bonisch tephras. Major- and trace-element compositions suggest these tephras represent six distinct high-silica magmas, with the Kohioawa tephras representing three distinct magma compositions that are atypical of the TVZ. The distribution of Kohioawa magma types (Types A, B, and C) changes through time, with the oldest deposits containing exclusively type A magma, the middle deposits containing types A and B, and the youngest deposits containing all three Kohioawa types. A combination of horizon-scale mineralogy and rhyolite-MELTS modeling suggest that only Kohioawa types B and C are saturated in sanidine – the presence of sanidine is atypical in Taupō Volcanic Zone magmas, but has been previously documented in the Whakamaru group ignimbrites. Rhyolite-MELTS geobarometry reveal similar shallow storage pressures (~50-150 MPa) for Kohioawa compositions. At least three different melt-dominated magma bodies sourced the Kohioawa tephras – these magma bodies were laterally juxtaposed and co-erupted for most of the Whakamaru eruptions. Magmas that preceded and post-dated the Whakamaru eruptions have more typical TVZ compositions, emphasizing the unique features of the Whakamaru system.

KEY WORDS

Whakamaru group ignimbrites; Kohioawa tephras; Taupō Volcanic Zone; Geobarometry; Glass; Ignimbrite; Magma storage; Tephra

INTRODUCTION

Understanding large, caldera-forming eruptions requires understanding eruptive magma bodies through space and time. While there is substantial work focused on the pyroclastic flow deposits of large eruptions (i.e., ignimbrites), the co-erupted pyroclastic fall deposits (i.e., tephras) can preserve important information that may be obscured in or not recorded by ignimbrites. For instance, the time-progression of eruptions may be poorly recorded in ignimbrites, but it is much more straightforward to constrain using the record in tephras.

Elucidating the pre-eruptive distribution and storage conditions of melt-dominated magma bodies is critical in our quest to understand how the crust can accommodate and erupt large volumes of magma (Charlier et al., 2007); Blundy and Cashman, 2008; Cashman and Giordano, 2014; Cooper and Kent, 2014; Wilson and Charlier, 2016; Gualda et al., 2018). For some magma systems, multiple melt-dominated magma bodies can erupt together (Gravley *et al.*, 2007; Cooper *et al.*, 2012; Gualda and Ghiorso, 2013; Bégué *et al.*, 2014a; Cashman and Giordano, 2014; Cooper, 2017; Swallow *et al.*, 2018; Gualda *et al.*, 2022), or from a single, zoned magma body as originally proposed for the Bishop Tuff (Hildreth, 1979) and for magma bodies that generally follow the mush model (Bachmann and Bergantz, 2004, 2008; Hildreth and Wilson, 2007; Deering *et al.*, 2011; Pamukçu *et al.*, 2013; Chamberlain *et al.*, 2015; Foley *et al.*, 2020). There is growing evidence suggesting that these melt-dominated magma bodies can be short-lived, lasting only centuries to a few millennia (Wilson and Charlier, 2009; Gualda *et al.*, 2012b; Cooper and Kent, 2014; Stelten *et al.*, 2014; Pamukçu *et al.*, 2015a; Gualda and Sutton, 2016; Allan *et al.*, 2017; Cooper *et al.*, 2017; Shamloo and Till, 2019); in contrast, the magma systems from which the melt-dominated magma is sourced can be active over timescales of tens to hundreds of thousands of years (Simon and Reid, 2005; Barboni *et al.*, 2015; Kaiser *et al.*, 2017; Reid and Vazquez, 2017).

The driving questions of this research to reconstruct pre-eruptive storage conditions of magmatic systems are:

1. How many melt-dominated magma bodies exist prior to large eruptions?
2. What are the storage depths of the melt-dominated magma bodies?
3. How do the number and depths of the melt-dominated magma bodies change through the lifecycle of a large magma system?

We focus on the Whakamaru magma system, which produced large, ignimbrite-forming eruptions in the central Taupō Volcanic Zone (TVZ), Aotearoa New Zealand (Ewart, 1965; Martin, 1965; Ewart and Healy, 1966; Briggs, 1976a, 1976b; Wilson *et al.*, 1986, 2009; Houghton *et al.*, 1995; Brown *et al.*, 1998). The Whakamaru group eruptions occurred after a ~200 ka hiatus in caldera-forming volcanism (Deering *et al.*, 2010), and their eruptions mark the beginning of an ignimbrite flare-up episode that lasted from ~350 to ~240 ka, during which at least six additional large (50-150 km^3 dense rock equivalent, DRE), caldera-forming eruptions occurred (Houghton *et al.*, 1995; Wilson *et al.*, 2009; Leonard *et al.*, 2010; Gravley *et al.*, 2016). The Whakamaru group eruptions are unique within the flare-up, as they are the largest eruptions by an order of magnitude (>2000 km^3 DRE) (Wilson *et al.*, 2009; Matthews *et al.*, 2012b; Gravley *et al.*, 2016) and contribute most of the erupted volume to the flare-up period (totaling >3000 km^3 DRE). They are atypically crystal-rich (up to ~40 wt% crystals), especially compared to other units in the TVZ (Brown *et al.*, 1998), and they have distinct mineralogical and textural attributes (Ewart, 1965; Brown *et al.*, 1998; Deering *et al.*, 2010; Gravley *et al.*, 2016). We thus focus on the development and eruption of the texturally and volumetrically unique magma system that kicked off an ignimbrite flare-up in one of the most active silicic systems in the world (Houghton *et al.*, 1995; Wilson *et al.*, 1995, 2009).

Deciphering how the melt-dominated magma bodies were organized in the crust and erupted through time is notoriously challenging for the Whakamaru magma system due to the complex field relationships and compositional signatures of the deposits (Brown *et al.*, 1998; Downs *et al.*, 2014). The Whakamaru group ignimbrites are divided into five mappable units (Figure 1) (Grindley, 1960; Martin, 1961, 1965; Healy *et al.*, 1964; Ewart and Healy, 1966; Briggs, 1976a, 1976b; Leonard *et al.*, 2010; Downs *et al.*, 2014); however, it is not yet clear how the eruption(s) relate to the mapped units (Briggs, 1976a, 1976b; Wilson *et al.*, 1986; Brown *et al.*, 1998). Ar-Ar ages of the Whakamaru group ignimbrites are indistinguishable at 349 ± 4 ka, with the exception of the later erupted Paeroa Subgroup at 339 ± 5 ka (Downs *et al.*, 2014), and the ignimbrite deposits do not overlap sufficiently in the field to definitively determine relative timing of the eruption(s) (Wilson *et al.*, 1986; Brown *et al.*, 1998).

Tephra deposited as pyroclastic fall deposits offers an opportunity to elucidate some of these issues (Bonadonna and Phillips, 2003; Folch and Felpeto, 2005; Brown *et al.*, 2012; Costa *et al.*, 2012; Houghton and Carey, 2015). The tephras exhibit clear relative ages since they are deposited sequentially.

In this work, we use detailed characterization of tephras from the Bay of Plenty (Aotearoa New Zealand), originally characterized by Manning (1995, 1996), to document in more detail the tephra packages that correlate with the Whakamaru group ignimbrites. We then use evidence from physical volcanology, glass compositions, and rhyolite-MELTS geobarometry to decipher how the melt-dominated magma bodies were organized in the crust, and how they erupted and changed through time.

Nomenclature

A note on nomenclature: We refer to ***magma*** as a geological material that includes melt (typically silicate in composition), but which can also include crystals and bubbles. A ***magma body*** is a parcel of magma that is in contact with rocks or other magmas, with clear boundaries. We can define melt-dominated magma bodies and magma mush bodies. A ***melt-dominated magma body*** is composed of crystal-poor magma that is readily eruptible and typically has a suspension of crystals and bubbles. A ***magma mush body*** is composed of crystal-rich magma that contains a framework of touching crystals, possibly with bubbles present. The magma mush is unlikely to be readily erupted. A ***magma type*** is a compositionally and texturally homogeneous group of magmas where a given magma type may be characteristic of a magma body, or it may be present in multiple magma bodies. The ***magma system*** includes all magma bodies through time.

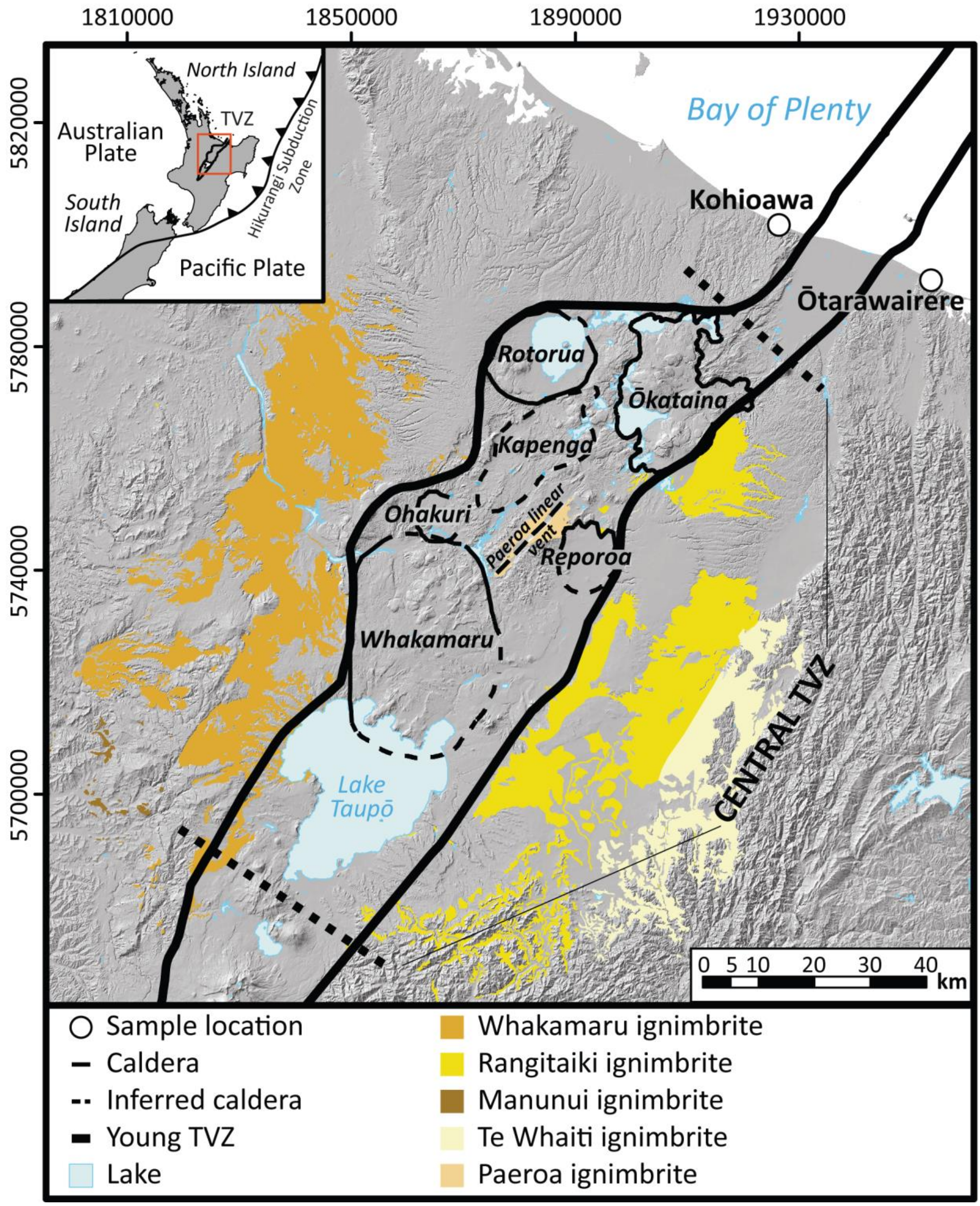

122 **Figure 1** Map of the Taupō Volcanic Zone (TVZ), New Zealand. The outline of the
123 young TVZ and major calderas of the most recent ignimbrite flare-up (~350-240 ka)
124 are shown. The Whakamaru caldera is the southernmost and largest caldera. The
125 locations of the two coastal tephra sequences, the Kohioawa section and Ōtarawairere

section, are marked with circles at the coast, ~90 km northeast of the caldera. Calderas are mapped after Leonard *et al*. (2010), outline of the young TVZ after Wilson et al. (1995), and the Whakamaru group ignimbrites are shown after Leonard *et al.* (2010), Brown *et al.* (1998), and Downs *et al.* (2014). Coordinate system is in meters in the New Zealand Transverse Mercator 2000 projected on the New Zealand Geodetic Datum 2000. The map inset shows the location of the TVZ within the North Island of New Zealand.

GEOLOGICAL BACKGROUND

The Taupō Volcanic Zone

The TVZ is a northeast-southwest rifted arc in the North Island of New Zealand (Figure 1) (Wilson *et al.*, 1995). The northern and southern ends of the TVZ produce predominantly andesitic eruptions, while the central TVZ is dominated by rhyolite eruptions with only minor amounts of dacite, andesite, and basalt (Wilson et al., 1984). The central TVZ is one of the most active silicic volcanic systems in the world (Houghton *et al.*, 1995; Wilson *et al.*, 1995), having produced at least 6000 km^3 of silicic magma over the last ~1.6 Ma (Wilson *et al.*, 2009), with silicic activity starting at ~1.9 Ma (Eastwood *et al.*, 2013; Chambefort *et al.*, 2014).

Over this time, there have been three ignimbrite flare-up periods in the TVZ, which were especially intense periods of ignimbrite-forming volcanism (Houghton *et al.*, 1995). The largest ignimbrite flare-up occurred from ~350 to ~240 ka (Houghton *et al.*, 1995; Gravley *et al.*, 2007, 2016; Wilson *et al.*, 2009), which erupted >3000 km^3 of magma from at least six calderas from a 90 x 40 km area of the central TVZ (see Figure 1; Gravley et al., 2016, and references therein). The Whakamaru group eruptions are the first of this ignimbrite flare-up, occurring at 349 ± 4 ka (Downs *et al.*, 2014). They discharged >2,000 km^3 of magma and are the largest eruptions in the young TVZ (Wilson *et al.*, 1986; Houghton *et al.*, 1995; Matthews *et al.*, 2012b; Downs *et al.*, 2014).

Although the Whakamaru group eruptions began the ignimbrite flare-up, they are distinct from the later eruptions of the period, as they have different textural and mineralogical signatures (Ewart, 1965; Briggs, 1976a, 1976b; Brown *et al.*, 1998; Deering *et al.*, 2010; Saunders *et al.*, 2010; Gravley *et al.*, 2016). They are relatively crystal rich (~15-40 wt% crystals) (Martin, 1961, 1965; Houghton *et al.*, 1995; Brown *et al.*, 1998), sometimes contain sanidine (which is very unusual in the TVZ) (Brown *et al.*, 1998; Downs *et al.*, 2014) and abundant hydrous phases (i.e. biotite and hornblende) (Ewart, 1965; Brown *et al.*, 1998), and are characterized by the presence of large quartz crystals (Briggs, 1976a, 1976b; Brown *et al.*, 1998; Saunders *et al.*, 2010; Matthews *et al.*, 2012a). The Whakamaru group ignimbrites are described as part of the “cold, wet, oxidizing” R1 type magma of Deering *et al.* (2010). In contrast, the later ignimbrite flare-up magmas erupted 50-150 km^3 at a time, are crystal poor (<10 wt% and sometimes <5 wt% crystals)(Gravley *et al.*, 2016), do not contain sanidine, and are generally part of the “hot, dry, reducing” R2 type magma of Deering *et al.* (2010). The Whakamaru group ignimbrites and the later-erupted flare-up ignimbrites thus represent the two geochemical types (R1 and R2, respectively) of silicic volcanism from the central TVZ (Deering *et al.*, 2010; Gravley *et al.*, 2016). The distinctions between the magmas imply potential differences in source and evolution of the magmas through time (Deering *et al.*, 2010; Gravley *et al.*, 2016; Gualda *et al.*, 2018).

Whakamaru group eruptions and their deposits

The Whakamaru group ignimbrites have most recently been Ar-Ar dated to 349 ± 4 ka, with the smaller Paeroa Subgroup ignimbrites (with a volume estimate on the order of 110 km^3) having slightly younger ages of 339 ± 5 ka (Downs *et al.*, 2014). The Whakamaru magma system had a complex history of magma generation (Saunders *et al.*, 2010) and of erupting multiple, distinct magma types (Brown *et al.*, 1998), potentially during one main eruption phase (with the exception of the younger Paeroa Subgroup) (Brown *et al.*, 1998; Downs *et al.*, 2014) or over multiple eruptive phases (Grindley, 1960; Martin, 1961; Wilson *et al.*, 1986; Houghton *et al.*, 1995). Zircon ages from the Whakamaru group eruptions show that there was an active magma system ~50-100 ka prior to eruption (Matthews, 2011), with older zircon ages implying that it was active up to ~250 ka prior to eruption (Brown and Fletcher, 1999), indicating a long history of maturation. Evidence from plagioclase and quartz show much shorter timescales (<300 a) for the final assembly, homogenization, and eruption (Saunders *et al.*, 2010; Matthews *et al.*, 2012a), which imply relatively short timescales for the ephemeral melt-dominated magma bodies consistent with what is seen elsewhere (Gualda *et al.*, 2012b; Pamukçu *et al.*, 2015b; Gualda and Sutton, 2016).

Within the Whakamaru group eruptions, the ignimbrites are distinguished from one another by differences in mineralogy, welding, and crystal content (Briggs, 1976a, 1976b; Wilson *et al.*, 1986, 1995; Brown *et al.*, 1998; Brown and Fletcher, 1999; Leonard *et al.*, 2010). Four widespread mappable ignimbrite units are described – the Whakamaru, Manunui, Rangitaiki, and Te Whaiti ignimbrites (Grindley, 1960; Healy *et al.*, 1964; Ewart, 1965; Martin, 1965; Ewart and Healy, 1966; Briggs, 1976a, 1976b), with the Paeroa Subgroup documented as a group of three younger ignimbrites derived from the same magma system but likely erupted from a separate source (Houghton *et al.*, 1995; Wilson *et al.*, 2009;

Leonard *et al.*, 2010; Downs *et al.*, 2014). The Whakamaru and Manunui ignimbrites are distributed to the west of the caldera, and the Rangitaiki and Te Whaiti ignimbrites are distributed to the east of the caldera (Figure 1). Wilson *et al.* (1986) propose that the Manunui and Te Whaiti ignimbrites could be correlative and erupted earlier, and that the Whakamaru and Rangitaiki ignimbrites could be correlative and erupted later. There is no documented significant time-break between the eruptions (Brown *et al.*, 1998; Downs *et al.*, 2014). In this work, we refer to the whole collection of ignimbrites as the Whakamaru group ignimbrites; Whakamaru ignimbrite refers to the specific ignimbrite *sensu stricto*.

Brown *et al.* (1998) reports four different compositional rhyolite pumice types (types A, B, C, D) from the erupted ignimbrites with some ignimbrites containing multiple pumice types. The lack of overlap of the ignimbrites in the field and the presence of multiple pumice types in the ignimbrites begs the question of how the melt-dominated magma bodies were stored in the crust and erupted through time. The characteristics of the magma types as described by Brown *et al.* (1998) are given in the supplementary data. Brown *et al.* (1998) interpret that the least evolved and hottest material likely erupted first, with sanidine only present in the later erupted, more evolved material. The presence of sanidine in the latter units is corroborated by drill core and field data (Martin, 1961, 1965; Ewart, 1965; Ewart and Healy, 1966; Briggs, 1976a).

The Rangitawa tephra (formerly the Mt. Curl tephra) has been suggested to be correlative with the Whakamaru group eruptions based on glass shard major-element compositions, ferromagnesian mineralogy, and similarity in paleomagnetic dates and zircon fission-track ages (Kohn *et al.*, 1992; Alloway *et al.*, 1993; Pillans *et al.*, 1996; Lowe *et al.*, 2001). The Rangitawa tephra is crystal-rich (Kohn *et al.*, 1992) and it is found across the North Island and as far away as the Chatham Islands (Holt *et al.*, 2010), as well as in offshore deposits (Matthews et al., 2012, and references therein). It has been interpreted to be related to a Plinian phase of the Whakamaru eruptions and is composed of type A magma (Brown *et al.*, 1998), which is predominant in the Whakamaru and Rangitaiki ignimbrites (Wilson *et al.*, 1986; Matthews *et al.*, 2012b). However, there is a caveat that fall deposits have never been documented in contact with the Whakamaru group ignimbrite sequence (Brown *et al.*, 1998). Therefore, these fall deposits can only be generally correlated to the Whakamaru group magma system via mineralogy and glass geochemistry.

Here, we compare Rangitawa tephra data (Matthews *et al.*, 2012b) and Whakamaru group ignimbrite data (Bégué *et al.*, 2014b; Gualda *et al.*, 2018) to the Kohioawa tephra (Manning, 1995, 1996) to investigate the correlation between Whakamaru magmas and the Kohioawa tephras and to elucidate the correlation and the pre-eruptive conditions.

Field relations and previous work

Tephras can be deposited much farther from the volcanic vents than material in pyroclastic density currents, and they can record important transitions in the eruption intensity (e.g., with changes in grain size, changes in ratios of ash, pumice, and lithics) (Bonadonna *et al.*, 2015; Houghton and Carey, 2015) and longer time-breaks between eruptions if soil horizons develop (Shoji *et al.*, 1994). The simple vertical organization of successive tephra units makes their relative age easy to determine, in contrast with the Whakamaru group ignimbrites. Manning (1995, 1996) correlates tephras across the eastern Bay of Plenty, including a sequence that he proposes to be correlative with the Whakamaru group eruptions. We use the formal names for the units within the tephra sequence from Manning (1995, 1996), focusing specifically on the Tablelands B-D, Paerata, Kohioawa, Murupara-Bonisch units. To understand the time-progressive evolution of the Whakamaru magma system, we focus on tephra deposits~90 km northeast of the caldera in the Bay of Plenty (Manning, 1995, 1996) (Figures 1-2).

Tablelands B-D

The Tablelands B-D tephras are the result of smaller volcanic events that precede the Paerata tephras that were interpreted to erupt from an Ōkataina volcanic center (Manning, 1995). The Tablelands B tephra (also known as the Ōtarawairere tephra after the type locality for this tephra unit) erupted a minimum estimate of 10 km^3 at ~380-390 ka (Manning, 1995). The Tablelands C and Tablelands D eruptions (~375 and 370 ka respectively) have a combined minimum volume estimated to be 2.5 km^3 (Manning, 1995).

Paerata

The Paerata tephra has a minimum volume estimate of 15 km^3 (Manning, 1995). The age is estimated to be ~370 ka, which is ~0-15 ka after the Tablelands B-D eruptions (Manning, 1995). The correlation of Paerata magma to the Whakamaru magma system is not clear, although Manning (1995) suggests that Paerata magmas could have been erupted from the Ōkataina volcanic center. Importantly, there is a well-developed paleosol at the top of the Paerata tephras, indicating a substantial time break before the eruptions that formed the Kohioawa tephras (Figure 2).

Kohioawa

The Kohioawa tephras are substantially thicker than other units, typically ~2-4 m in the Bay of Plenty, and are subdivided into four subunits (Manning, 1995), described below and in Tables 1 and 2. They are estimated to be ~350 ka in age (Manning, 1995). From glass geochemistry, Manning (1995) recognizes two distinct chemical populations of glass where one of the Kohioawa tephra glass types is correlated with that recorded in the widespread Rangitawa tephra.

Murupara-Bonisch

The Murupara-Bonisch tephras post-date the Kohioawa tephras and precede the Matahina ignimbrite-forming eruption (322 ± 7 ka; Leonard *et al.*, 2010), which is observed overlying these tephras at the Kohioawa section (Figure 2a) (Manning, 1995, 1996). The Murupara and Bonisch tephras erupted at ~340-330 ka and have a combined volume of ~50 km^3 (Manning, 1995, 1996). Both the Murupara-Bonisch and the subsequent Matahina ignimbrite (Bailey and Carr, 1994) are interpreted to have erupted from the Ōkataina volcanic center (Manning, 1995, 1996). The Matahina ignimbrite is the next large eruption in the flare-up period, having erupted ~150 km^3 DRE (Bailey and Carr, 1994) of magma at 322 ± 7 ka (Leonard *et al.*, 2010). The Matahina ignimbrite has magmatic characteristics of both R1 type (typified by the Whakamaru group eruptions) and R2 type (typified by the later flare-up magmas) (Deering *et al.*, 2010).

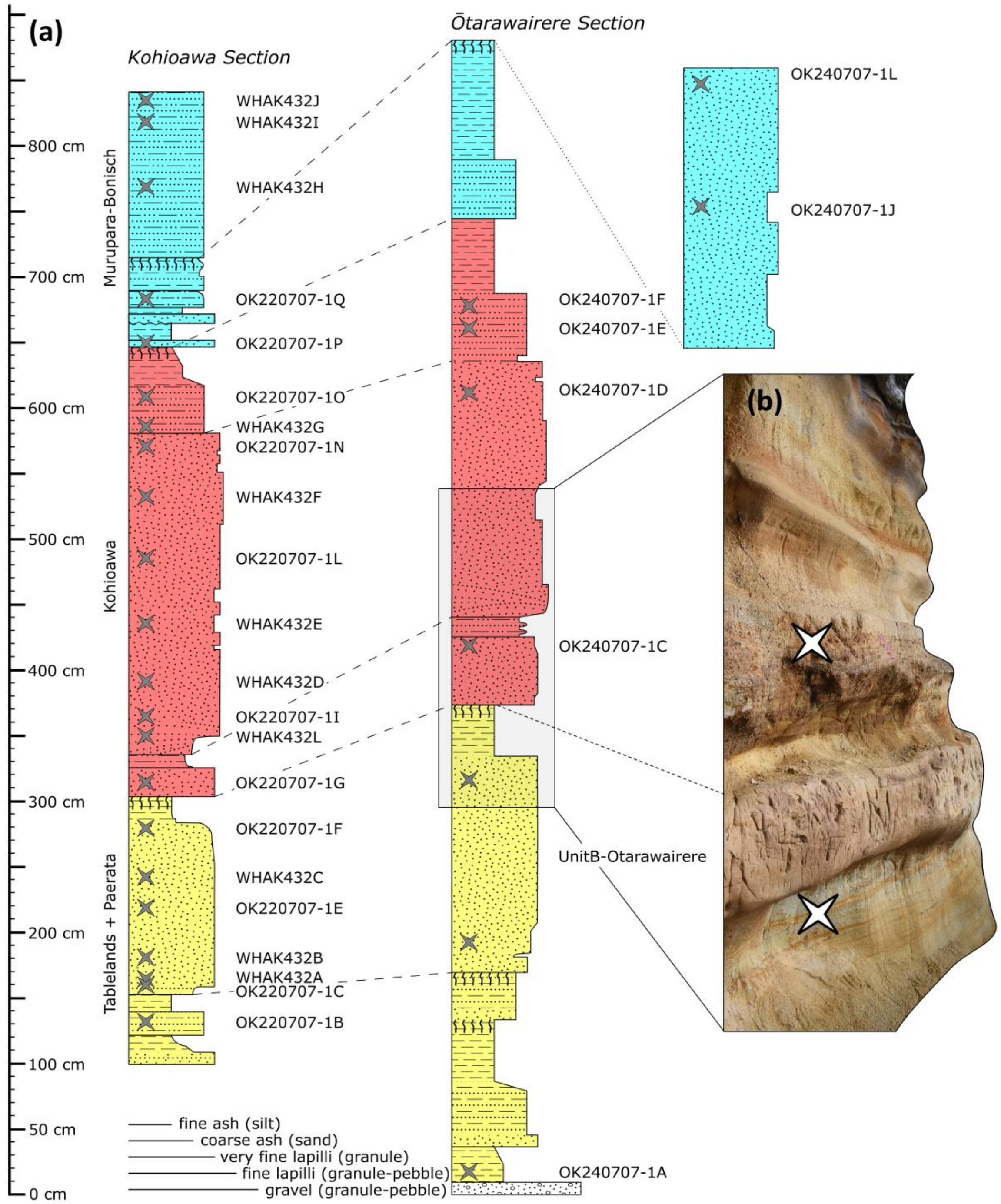

Figure 2 a) Schematic section of the two tephra sequences (Kohioawa and Ōtarawairere) studied in this work and (b) a field photo of a portion of the Ōtarawairere tephra sequence. In a), the width of the units in the schematic corresponds to grain size. The patterns follow the Federal Geographic Data Committee Digital Cartographic Standard for Geologic Map Symbolization (FGDC-

STD-013-2006). The paleosols are denoted by vertical wiggly lines, which do not extend through entire packages to enhance readability and because the thicknesses of the paleosols often vary across an exposure. Measured thicknesses of paleosols are provided in Table 2. The 22 samples from Kohioawa section and 8 samples from Ōtarawairere section are marked with gray X's and labeled. Note that the sample "UnitB-Ōtarawairere" in the Ōtarawairere section was sampled as a mixture of tephra from the top and bottom of this horizon, marked by X's. Correlations between units in the Kohioawa and Ōtarawairere sections are marked with dashed lines. For readability, the top of the Ōtarawairere section is shown at the top right of the figure, as indicated by the dotted line. The yellow basal units comprise the Tablelands and Paerata unit; the red middle unit is the Kohioawa unit; the top light-blue unit is the Murupara-Bonisch unit. Note that the Kohioawa unit is subdivided into three subunits, as indicated by the dashed lines. A general description of the units is found in Table 1; a detailed description of each horizon is found in Table 2. (b) The field photo shows a part of the Ōtarawairere section (from ~300 cm to ~600 cm, as indicated by the light gray box). This photo highlights the transition from the Paerata unit to the Kohioawa unit. These units are separated by a thick paleosol, the top of which is marked by a dotted line. Two of the sample locations are marked by X's where the lower X corresponds to sample UnitB-Ōtarawairere, and the upper X corresponds to sample OK240404-1C. The cliff-like nature of the Kohioawa sequence precludes taking equivalent photos of that outcrop.

METHODS

Field observations and sampling

We focus our study at two locations where Manning (1995, 1996) characterized the relevant sequences of tephras exposed in the Bay of Plenty: the Kohioawa section and the Ōtarawairere section (Figures 1-2). The Kohioawa section is ~4 km west-northwest of Matatā, along State Highway 2(37°52'27.25"S, 176°42'40.85"E). The Ōtarawairere section is along the Kohi Point Scenic track at the northwest end of Ōhope Beach (37°57'11.80"S, 177° 1'26.20"E). The two locations are ~30 km apart along the coast, and ~90 km northeast of the Whakamaru caldera (Figure 1). Each section was described and sampled during two field seasons in 2007 (samples labeled OK220707 and OK240707) and 2017 (samples labeled WHAK432), when we collected ~1 kg of bulk tephra from horizons within the four units (Tablelands B-D, Paerata, Kohioawa, and Murupara-Bonisch). Bulk tephra was sampled from horizons where: (1) distinct changes or differences in characteristics of the tephra material were observed; (2) above and below paleosols; and (3) where fresher tephra was available.

We documented and sampled the Kohioawa section in detail over 670 cm with an additional three samples and more limited observations collected from the upper section between 670 and 730 cm. The base of the Kohioawa section is measured from the distinct, but not sharp, boundary near the top of the Kohioawa cliffs, where the tephras outcrop above the sandy and vegetated slope. We sampled a total of 22 horizons at the Kohioawa section. The Ōtarawairere section was similarly documented over 1095 cm. The base is measured from the obvious basal gravels. The sampling of the Ōtarawairere section was sparser, with 8 horizons sampled. The two sections are correlated using paleosols, grain size, and horizon thickness (Figure 2).

Horizon characterization

In addition to the sedimentological and mineralogical observations made in the field, a few key horizons were mineralogically characterized in the laboratory. Mineral componentry was conducted on several of the horizons from the Kohioawa section – OK220707-1B (Tablelands D tephra); OK220707-1C (Paerata tephra); OK220707-1E, OK220707-1G, OK220707-1I, OK220707-1L, OK220707-1O (Kohioawa tephra); OK220707-1P, OK220707-1Q (Murupara-Bonisch tephra). Particular attention to the felsic assemblage (including the presence of sanidine) was conducted on horizons OK220707-1G, OK220707-1I, OK220707-1L, OK220707-1O, OK220707-1Q.

Five to six pristine, generally larger coarse-ash sized to fine-lapilli sized pumice clasts from each horizon were chosen for determination of major and trace-element glass compositions. Most chosen clasts are 0.01-0.03 cm^3 (~0.15 cm diameter), although clast sizes vary between horizons. The chosen clasts were the largest size fraction per horizon. We focused on individual clasts because they represent individual parcels of magma that erupted but did not fully fragment. A total of 153 clasts were analyzed in this study for major- and trace-element compositions. Each clast was mounted in epoxy for glass analysis.

Unfortunately, due to their small sizes, it is impractical to determine the mineralogy of each individual clast, as the total area exposed for each clast is unlikely to be representative of the mineralogy of the entire clast. Instead, we focus on the mineralogy of each horizon, which obscures potential differences in mineralogy between magma types present in the same horizon (particularly for horizons within the Kohioawa unit, for which some of the types are sanidine-bearing, while others are sanidine-free). To further document the presence or absence of sanidine in individual horizons, an additional 3-5 clasts were chosen per horizon to check for the presence of sanidine in every horizon. Each clast was carefully crushed with a soup spoon to preserve the intact minerals and was placed on a glass slide with 1.544 refractive index oil (sanidine was identified by its negative optical relief and tabular habit, which contrast with the positive optical relief of plagioclase and quartz).

Glass geochemistry

Glass major-element compositions were obtained at Vanderbilt University using an Oxford X-max 50-mm^2 Energy Dispersive Spectrometer (EDS) attached to a Tescan Vega 3 LM Variable Pressure Scanning Electron Microscope (SEM). Most glass analyses were obtained using 15 kV accelerating voltage (with several obtained with an accelerating voltage of 18-20 kV to achieve a higher output count rate) and a specimen current of ~2 nA at a working distance of 15 mm. The USGS-Rhyolite Glass Mountain (RGM-1) standard was measured at the beginning of each SEM session as a secondary standard. Data reduction for all SEM-EDS analyses was performed using the Aztec Oxford software, which uses internal standards for calibration. Results from the USGS RGM-1 standard are provided in the supplementary data. Pamukçu *et al*. (2015b, 2021) show that the quality of glass analyses obtained with SEM-EDS at Vanderbilt University are comparable to or better than results obtained at other labs with the electron probe microanalyzer (Reed and Ware, 1973; Ritchie *et al.*, 2012).

Per clast, we analyzed ~15 spots of the largest, most pristine sections of glass, far from crystals. We calculate the average composition of each clast and report the mean with the associated standard deviation. We routinely find that the uncertainty deriving from the external reproducibility (i.e., uncertainty deriving from the variability of analyzing multiple spots) is larger than the analytical uncertainty for most major elements (derived from counting statistics from a single analysis), such that the mean and standard deviation of multiple analyses better represents the composition of the analyzed glass than a single analysis would. Analyses were excluded from the average if: 1) a mineral (usually feldspar or a Fe-Ti oxide) was encountered; 2) the SiO_2 was >82 wt%, which likely indicates silicification of the glass; 3) the composition of individual elements was outside 1.5 times the interquartile range (IQR) for that individual clast, which likely indicates glass alteration. This IQR test was performed once, and not iteratively, to identify and remove analyses that fall outside the natural variability of the glass. We manually inspected the spot compositions from each clast for evidence of multiple compositional populations within the clast (e.g., from mingling or alteration).

Glass trace-element compositions were obtained via Laser Ablation Inductively Coupled Plasma Mass Spectrometry (LA-ICPMS) at Vanderbilt University using a Photon Machines Excite 193 nm excimer laser attached to a Thermo iCAP Q quadrupole ICPMS system. For each analysis, a 50 µm × 50 µm square laser spot size was ablated for 25 s at a pulse frequency of 10 Hz. NIST 610 was used as the primary standard and NIST 612 and RGM-1 were used as secondary standards. ^{28}Si was used as an internal standard, using the average SiO_2 content determined for each lapillus sample by SEM-EDS analysis prior to trace-element analysis. Concentrations were processed through the data reduction program Glitter (van Achterbergh *et al.*, 2001; Griffin *et al.*, 2008).

Similar to the EDS-SEM procedure, we analyzed ~15-20 spots per clast for trace-element compositions using LA-ICPMS, where the spot locations were not the same as those analyzed for major-element compositions by EDS-SEM. We again calculate averages for each clast, and the standard deviation of a measure of uncertainty. Individual trace-element analyses were discarded if: 1) a mineral (usually feldspar or a Fe-Ti oxide) was encountered;

2) or if an analysis had at least 5 elements below the detection limit; individual analytes were discarded if they failed the same IQR method as the major element data; clasts were not considered further if <3 spots provided adequate compositional analyses for a given clast.

Comparison with Rangitawa tephra, Whakamaru ignimbrite, and TVZ glass compositions

To test the correlation between Kohioawa tephras with Whakamaru group ignimbrites and the Rangitawa tephras, we compare our tephra glass compositions to published TVZ ignimbrite and tephra glass compositions from the literature. We compare our glass data to the Whakamaru ignimbrite compositions (Gualda *et al.*, 2018); to the Rangitawa tephra, which has been previously correlated to the Whakamaru ignimbrites and Kohioawa tephra (Manning, 1995, 1996; Matthews *et al.*, 2012b); and to other TVZ flare-up glass major-element (Bégué *et al.*, 2014b; Gualda *et al.*, 2018) and trace-element data (Gualda *et al.*, 2018).

Geothermometry

Zircon saturation temperatures were calculated using the mean glass compositions of the individual clasts using the formulations of Watson and Harrison (1983) and Boehnke et al. (2013). Both formulations are based on the major elements and Zr concentration in the glass. If the melt is saturated in zircon, the temperature represents the temperature of zircon-melt equilibrium (likely a pre-eruptive storage temperature; see, for instance, t if the melt is undersaturated in zircon, the calculations return a minimum temperature. Uncertainties were calculated using the standard deviation of the Zr content of an individual clast. While there are uncertainties propagated via major-element composition, the impact on the zircon saturation temperature is minimal due to the minor role of the major-element composition in the calculation.

Geobarometry

Thermodynamic modeling was conducted using rhyolite-MELTS (Gualda *et al.*, 2012a; Gualda and Ghiorso, 2015). We used the rhyolite-MELTS geobarometer (Gualda and Ghiorso, 2014) to determine the pressure at which certain mineral phases are in equilibrium with the input major-element glass composition. The glass composition is a proxy for the melt composition, which is assumed to be in equilibrium with the observed crystallizing mineral assemblage. We use the observed mineralogy in the horizons to constrain the phases potentially in equilibrium with the melt; in particular, quartz and plagioclase are ubiquitous in all units, and suggest equilibration between melt, plagioclase, and quartz. It has been previously demonstrated (Bégué *et al.*, 2014b; Gualda and Ghiorso, 2014; Pamukçu *et al.*, 2015b; Harmon *et al.*, 2018) that rhyolite-MELTS geobarometry is effective in identifying situations in which glass compositions do not record equilibrium conditions. This geobarometry method retrieves pre-eruptive storage conditions, and we focus on the pre-eruptive storage pressures to determine the depths of the magma bodies (Gualda and Ghiorso, 2013, 2014; Bégué *et al.*, 2014b; Pamukçu *et al.*, 2015b; Harmon *et al.*, 2018; Gualda *et al.*, 2022).

As discussed above, the coarse ash-lapilli clasts are too small for us to unequivocally determine their mineral assemblages by direct observation, in particular the presence or absence of sanidine. We leverage the results of our rhyolite-MELTS pressure calculations to infer whether or not the glass composition is consistent with sanidine saturation, in addition to plagioclase and quartz, in the individual clasts. We thus consider two potential assemblages:

1. quartz+plagioclase (qtz-1feld)

2. quartz+plagioclase+sanidine (qtz-2feld)

If a rhyolite-MELTS pressure calculation yields a qtz-2feld result, we conclude that such melt composition was very likely in equilibrium with sanidine. We emphasize that this does not affect the pressure calculation, given that – in this case – the qtz-1feld solution would be the same as the qtz-2feld pressure, with the advantage that qtz-2feld pressures have a smaller error than qtz-1feld pressure (see Gualda and Ghiorso, 2014). In Figure 3, we show examples of calculations that yield qtz-1feld (no sanidine), qtz-2feld (sanidine-bearing), and no solution (glass composition does not record equilibrium between melt, quartz, and feldspars). For some compositions, the quartz and plagioclase curves become coincident or nearly so at pressures of 100 MPa or less. In these cases, we follow the method of Bégué *et al.* (2014) and report the maximum pressure for which the difference between the two saturation curves is ≤ 5 °C. These pressures are therefore reported as 50, 75, or 100 MPa depending on the pressure at which the two curves begin their coincident relationship and should be interpreted as maximum pressure estimates (Bégué *et al.*, 2014).

We calculated pressures for mean glass compositions of all clasts (153 compositions after several clasts were discarded and some clast glass compositions were subdivided). Following previous work (particularly (Bégué *et al.*, 2014b; Gualda and Ghiorso, 2014; Pamukçu *et al.*, 2015b), we model from the liquidus to >90 wt% crystals, 500-25 MPa in 25 MPa steps, and 1100-700 °C in 1 °C steps. We set all MnO and P_2O_5 values to 0. If MgO was reported to be 0 wt% from the SEM-EDS data, we interpret that the MgO value is below the detection limit from the EDS analysis. Rhyolite-MELTS calculations cannot be performed with MgO equal to zero, given that it would set the activity of MgO (a_{MgO}) to zero – rhyolite-MELTS is optimized for natural compositions, in which a_{MgO} is never zero. To correct this, we input the detection limit of 0.05 wt% MgO in the cases where MgO was reported as 0 wt%. Because this only affects the stability of mafic minerals, it has no impact on the pressure calculations presented here. We assume H_2O saturation (we input 10 wt% H_2O to assure saturation at all conditions – any H_2O in excess of saturation does not impact rhyolite-MELTS calculations) and oxygen fugacity (f_{O2}) equal to NNO. Gualda and Ghiorso (2014, 2015) demonstrate that pressures for assemblages involving quartz, plagioclase, and sanidine are insensitive to H_2O and f_{O2}. Further, because we focus on pressures involving only quartz and feldspars, the inability of rhyolite-MELTS to appropriately model amphiboles has no impact on our calculated pressures. For a full description of the geobarometer, see Gualda and Ghiorso (2014)

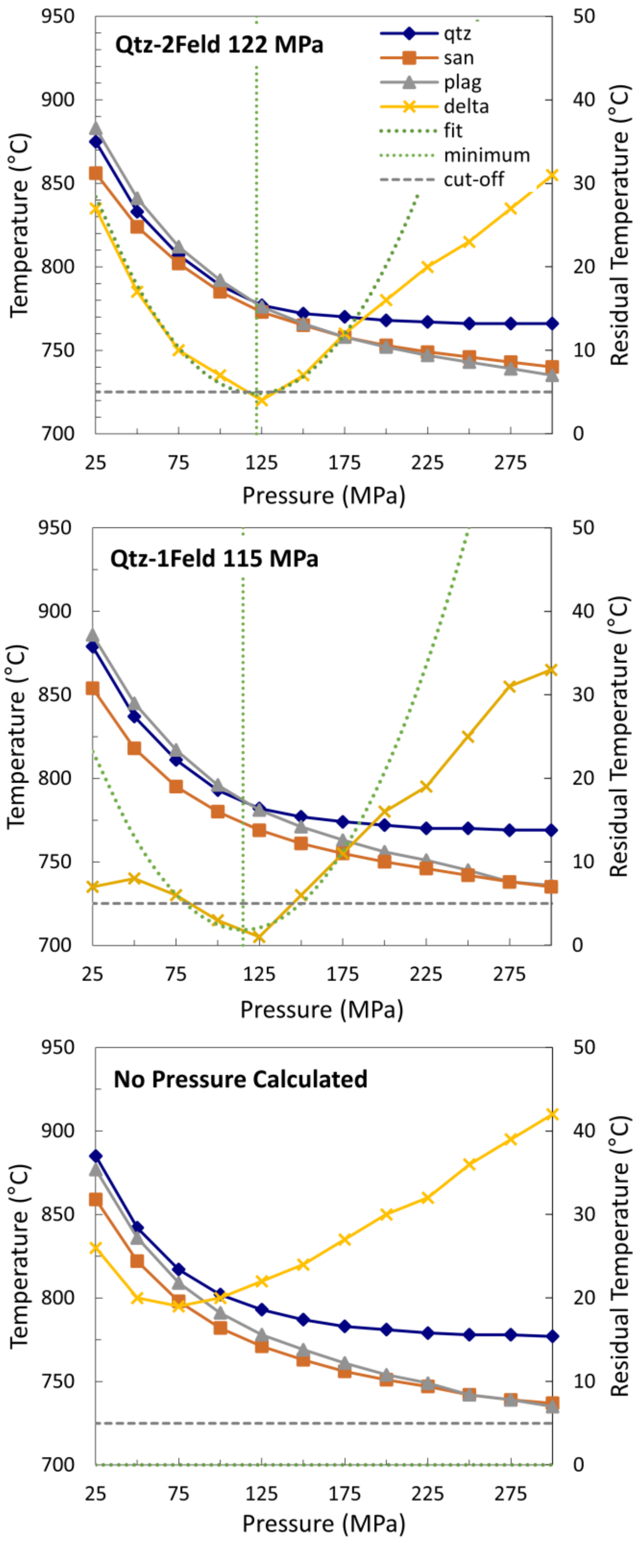

Figure 3 Representative Rhyolite-MELTS geobarometry calculations, which represent the conditions of magma storage prior to eruption. For all panels, the

saturation surfaces of quartz, sanidine, and plagioclase are plotted in temperature (left vertical axis) vs pressure (x-axis) space. The saturation surface of a given mineral represents the highest temperature (as a function of pressure, in this diagram) at which a mineral is stable. If melt of the given composition equilibrated with the inferred mineral assemblage, the saturation surfaces will intersect at the temperature and pressure of equilibration. The difference between the mineral phases' saturation temperatures at a given pressure are represented by the yellow "delta" line (right vertical axis). In the top panel, all three mineral phases saturate within 5 °C at 125 MPa (i.e., the residual temperature, represented by the delta line, has a minimum equal to or less than 5 °C, represented by the gray dashed "cutoff" line), so a qtz-2feld pressure is calculated. The pressure is calculated by fitting a parabola to the minimum residual temperature and the two points above and below the minimum pressure (green dashed "fit" parabola). The minimum of the parabola represents the calculated storage pressure of 122 MPa (green dotted vertical line in the top panel). In the middle panel, the difference between the saturation surfaces of the three mineral phases is greater than 5 °C, but the difference between the quartz saturation surface and one of the feldspars is equal to or less than 5 °C at a pressure near 125 MPa, so a qtz-1feld storage pressure is calculated (115 MPa). If the residual temperature of the saturation surfaces is greater than 5 °C, then no pressure is calculated, as shown in the bottom panel. Note that in the middle panel, the plagioclase and sanidine curves cross at ~300 MPa. This is an invalid pressure as the quartz saturation surface is at a higher temperature than the plagioclase-sanidine intersection. This indicates that the plagioclase-sanidine intersection would not be in equilibrium with the input glass composition. We perform this calculation on all average clast glass compositions to determine the storage pressures. When qtz-2feld solutions are calculated, we infer that melt equilibrated with an assemblage containing sanidine; similarly, when only a qtz-1feld solution is found, we infer that the melt did not equilibrate with sanidine. The clast compositions used for these examples are WHAK432D-4, WHAK432D-3, and WHAK432E-1, from top to bottom

RESULTS

Field observations

We focus on the four units – the Tablelands B-D, Paerata, Kohioawa, and Murupara-Bonisch units from Manning (1995) – the boundaries of which are defined by paleosols or distinct changes in physical volcanological characteristics. There are three loess paleosols described at the Kohioawa section and four loess paleosols described at the Ōtarawairere section Manning (1995). At the Kohioawa section, the paleosols mark the boundaries between the Paerata and Kohioawa units, between the Kohioawa and Murupara-Bonisch units, and a boundary within the Murupara-Bonisch unit. At the Ōtarawairere section, a paleosol between Tablelands C and Tablelands D horizons and the thickest paleosol (~20-40 cm, although the thickness varies across the outcrops) marks the break between the Paerata and Kohioawa units. There is no discernible paleosol between Kohioawa and Murupara-Bonisch units at the Ōtarawairere section (Figure 2a).

At both locations, the deposits are characterized by laterally continuous, mostly horizontal layers that can be traced for 10s of m. The exposure is divided into horizons that range mostly from ~1 cm to ~20 cm, and the thickest three horizons at each location are >1 m thick. The horizons are composed of mostly clast-supported, fine-grained volcanic material that ranges from orange-yellow to light-yellow to gray in color. Generally, the grain size within a specific horizon is consistent, although grain size varies from clay/ash-sized to very coarse sand-sized over the different horizons within the exposures. The make-up of the material is predominantly juvenile volcanic pumice clasts, a variable amount of smaller volcanic lithics and loose crystals, and sometimes a sandy matrix that indicates post-depositional water interaction (Manning, 1995). A general description of each unit is in Table 1; a detailed log of each horizon, including grain size, observed mineralogy, and paleosols is given in Table 2; a schematic of the outcrops is shown in Figure 2a.

Tablelands B-D

The lowest horizons comprise the Tablelands B-D unit. At the Kohioawa section, the tephras described are the Tablelands C and D tephras; the tephra sampled is the Tablelands D tephra (sample OK220707-1B). At the Ōtarawairere section, the tephras described are the Tablelands B, Tablelands C, and Tablelands D tephras; the tephra sampled is the Tablelands B tephra (OK240707-1A), which sits atop weathered gravels.

Paerata

The Paerata unit is present at both locations. This unit is defined by a coarse-grained, massive horizon and a thick paleosol at the top of the unit, which is ~20 cm thick at the Kohioawa section. At the Kohioawa section, samples are WHAK432A, WHAK432B, OK220707-1E, WHAK432C, OK220707-1F. At the Ōtarawairere section, the sample UnitB-Ōtarawairere is a mixture of pumice from near the base and near the top within the Paerata unit, marked in Figure 2.

Kohioawa

The Kohioawa unit can be divided into three main packages, shown by the dashed lines in Figure 2a. The lowest Kohioawa package is predominantly massive and grain supported, with a finer horizon on top (samples OK220707-1G at the Kohioawa section and sample OK240707-1C at the Ōtarawairere section). Manning (1995) subdivided this lowest package into two subunits, as noted by a thin solid line in Figure 2a. The middle Kohioawa package contains one horizon, which is the thickest horizon of the outcrops (samples WHAK432L, OK220707-1I, WHAK432D, WHAK432E, OK220707-1L, WHAK432F, OK220707-1N at the Kohioawa section and OK240707-1D at the Ōtarawairere section). There are cross-beds observed at the basal ~25 cm of this horizon. The rest of this horizon is massive and is coarser grained than the rest of the horizons in the outcrops. It is composed of predominantly ash sized to fine-lapilli sized juvenile clasts, crystals, and lava lithics. The top package, in contrast, has alternating ~3 cm thick horizons of coarse ash and grain-supported, very fine lapilli clasts (samples WHAK432G, OK220707-1O at the Kohioawa section and OK240707-1E, OK240707-1F at the Ōtarawairere section). These horizons then grade into a thick developed paleosol in the Kohioawa section, which marks the top of this unit.

Murupara-Bonisch

The fourth unit, which contains the Murupara-Bonisch horizons, shows alternating horizons between coarse and fine-grained material that becomes distinctly more friable and sandier than the rest of the outcrop (samples OK220707-1P, OK220707-1Q, WHAK432H, WHAK432I, WHAK432J at the Kohioawa section and OK240707-1J, OK240707-1L at the Ōtarawairere section). Due to the cliff-like outcrop, observations and sampling are more difficult, so this unit is not as well documented. The uppermost horizons are finer grained and comprise a thick (>1 m) ash deposit at the top of the outcrops. At the Kohioawa section, the Matahina ignimbrite overlies the Murupara-Bonisch unit.

Mineralogy

Mineralogy was described and recorded at the horizon scale through the sequence in the field and via SEM-EDS. Plagioclase, quartz, hornblende, orthopyroxene, and Fe-Ti oxides are the main phases present in all horizons analyzed. Biotite is observed in the middle section in samples OK220707-1I, OK220707-1L, OK220707-1O, OK220707-1P. Results are summarized in Table 2.

The felsic mineral componentry reveals that the first package of the Kohioawa unit (sample OK220707-1G) is the only horizon in the Kohioawa unit that does not contain sanidine. We do not observe sanidine in the other units (Tablelands B and D, Paerata, and Murupara-Bonisch units).

Glass compositions

In most of the 153 clasts, the major elements show a single composition; however, there are 14 clasts for which we subdivided the glass analyses into two populations. There is one additional clast in which we subdivided the glass into three different populations. There were no subdivisions of glass data for the Tablelands B and Tablelands D clasts, 2 subdivisions in the Paerata clasts (subdivisions for 5% of clasts), 7 subdivisions in the Kohioawa clasts (subdivisions for 9% of clasts), and 6 subdivisions in the Murupara-Bonisch clasts (15% of the clasts). In all units, it is a minority of clasts that exhibit multiple glass compositions. Of the 15 clasts that were subdivided into multiple compositions, 7 of them were later found to be small accretions of ~two ash clasts and sediment. Those 7 clasts were discarded from further analysis. Five of those clasts were from Kohioawa samples, and 2 were Murupara-Bonisch clasts; consequently, the percentages of clasts with subdivisions decreases to 2% for Kohioawa clasts and 10% for Murupara-Bonisch clasts.

All compositional data are reported as the mean and 1 standard deviation of individual clasts, with subdivisions denoted by "-A" or "-B" for the clasts with multiple populations.

We define six compositional groups using major- and trace-element compositions. The major-element compositions show that glasses in all clasts are high-silica rhyolites with 76.0-78.5 wt% SiO_2. Na_2O and K_2O are negatively correlated for all types, which could indicate some degree of Na-K exchange. The full data set of mean and standard deviation values of major and trace elements is reported in the supplementary data. The different geochemical characteristics of the Kohioawa glass compositional groups are defined and detailed in Table 3 and in Figures 4-6. The six compositional types are defined as follows:

Tablelands B, Tablelands D, and Paerata type

The first compositional type comprises glasses from the Tablelands B, Tablelands D, and Paerata clasts (labeled Tablelands + Paerata in Figures 4-6). This type is defined by relatively high CaO (>~1.0 wt%) and low K_2O (<~4.0 wt%) in major elements (Figure 4) and low Rb (110-140 ppm) and Cs (4-5 ppm) in the trace elements (Figure 5). These clasts have the highest Ba and the lowest LREE abundances of all types.

Kohioawa types

The Kohioawa clasts exhibit three glass compositional types, which appear throughout the Kohioawa tephra deposits. Together, the Kohioawa types are the lowest in CaO and highest in K_2O of all glasses analyzed (Figure 4). Kohioawa types are higher in Rb, lower in Sr, and lower in Eu when compared to the other types (Figure 5).

The Kohioawa glass compositions can be subdivided into types A, B, and C, where types B and C are more similar. Type A can be distinguished clearly from types B and C by CaO and TiO_2, and by Mn, Sr, and Ba. It can be subtly distinguished by MgO and FeO, and by Cs, Zr, Eu, and Yb. There are no clear trends in SiO_2 and Al_2O_3. There are very subtle trends in many of the trace elements, but we highlight only those that have strong signatures. The rare earth element (REE) values can also distinguish type A from types B and C.

Types B and C are similar but can be subdivided on the basis of Ba contents. They can also be subdivided subtly in CaO and SiO_2, and by Sr, Eu, U, and Pb. Kohioawa types B and C are similar to one another but are compositionally distinct from all other types in this study, with little to no overlap with the other types in trace-element compositions (e.g., Rb, Sr, Eu, Ba), Figures 5-6. The quantitative trends to distinguish tephra types are provided in Table 3. Kohioawa type A is the only type present in the lowest Kohioawa package. In the middle package, both Kohioawa types A and B are present. In the upper Kohioawa package, Kohioawa types A, B, and C are all present, although Kohioawa type C is the dominant glass type we analyzed (Figures 7-8). There are 4 clasts that do not clearly fall into the three Kohioawa groups. These are referred to as “undefined” and are not discussed further in this paper.

Murupara-Bonisch types

The Murupara-Bonisch clasts can be subdivided into two compositional types. The Murupara-Bonisch type A has lower SiO_2 and higher CaO (average ~1.2 wt%) and FeO (average ~1.4 wt%) than all other types (Figure 4). The Murupara-Bonisch type B overlaps with the Kohioawa type A for CaO (average 0.8 wt%) and SiO_2 (average 77.7 wt%) but differs in other elements (Figure 5). Note that in some trace elements, the Tablelands B, Tablelands D, and Paerata type often overlaps with the Murupara-Bonisch type A (e.g., Cs and Nd), but that is not a ubiquitous characteristic, and the Tablelands B, Tablelands D, and Paerata type is distinguishable from both Murupara-Bonisch types, e.g., Ba (Figure 5). The Murupara-Bonisch type A is not present in the clasts from the first Murupara-Bonisch horizon, and it is the only type seen in the final two Murupara-Bonisch horizons (Figures 7-8).

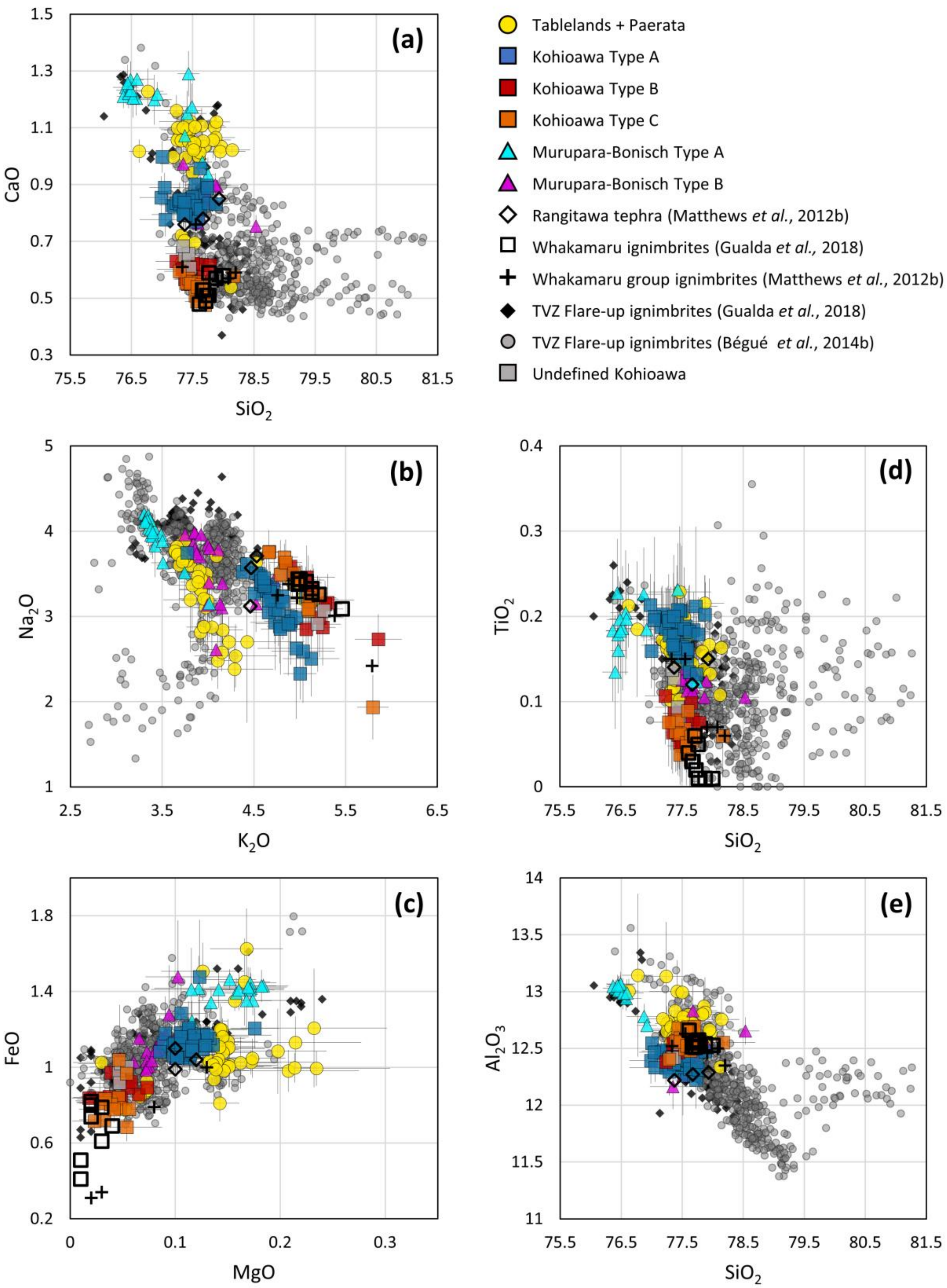

Figure 4 Major-element compositions of glass from clasts of the Kohioawa and Ōtarawairere sections in a) CaO vs. SiO_2; b) Na_2O vs. K_2O; c) FeO vs MgO; d) TiO_2

vs SiO_2; and e) Al_2O_3 vs SiO_2 space, reported as wt% of each oxide. There is one group for the Tablelands and Paerata unit represented by yellow circles; three groups for the Kohioawa unit represented by blue, red, and orange squares; and two groups for the Murupara-Bonisch unit represented by cyan and magenta triangles. We report one standard deviation of each clast, represented by gray error bars. We include literature data: 1) Rangitawa tephra data Matthews *et al.* (2012b), represented by open black diamonds; 2) Whakamaru ignimbrite data from Gualda *et al.* (2018), represented by open black squares, and from Matthews *et al.* (2012b), represented by black crosses; 3) ignimbrite data from the TVZ from other ignimbrite flare-up eruptions from Gualda *et al.* (2018), represented by black diamonds, and from Bégué *et al.* (2014b), represented by gray circles. In panels a and b, there is one composition from Bégué *et al.* (2014b) that is excluded (with 74.8 wt% SiO_2 and 0.65 wt% CaO) to improve readability of the data. There are four “undefined” compositions from the Kohioawa tephras that do not fall into the three Kohioawa types, represented by gray squares. Note that Kohioawa types B and C show the lowest CaO, MgO and Fe; Kohioawa glasses have higher K_2O than other units; SiO_2 values are similar for most tephra glasses, except for Murupara-Bonisch type A.

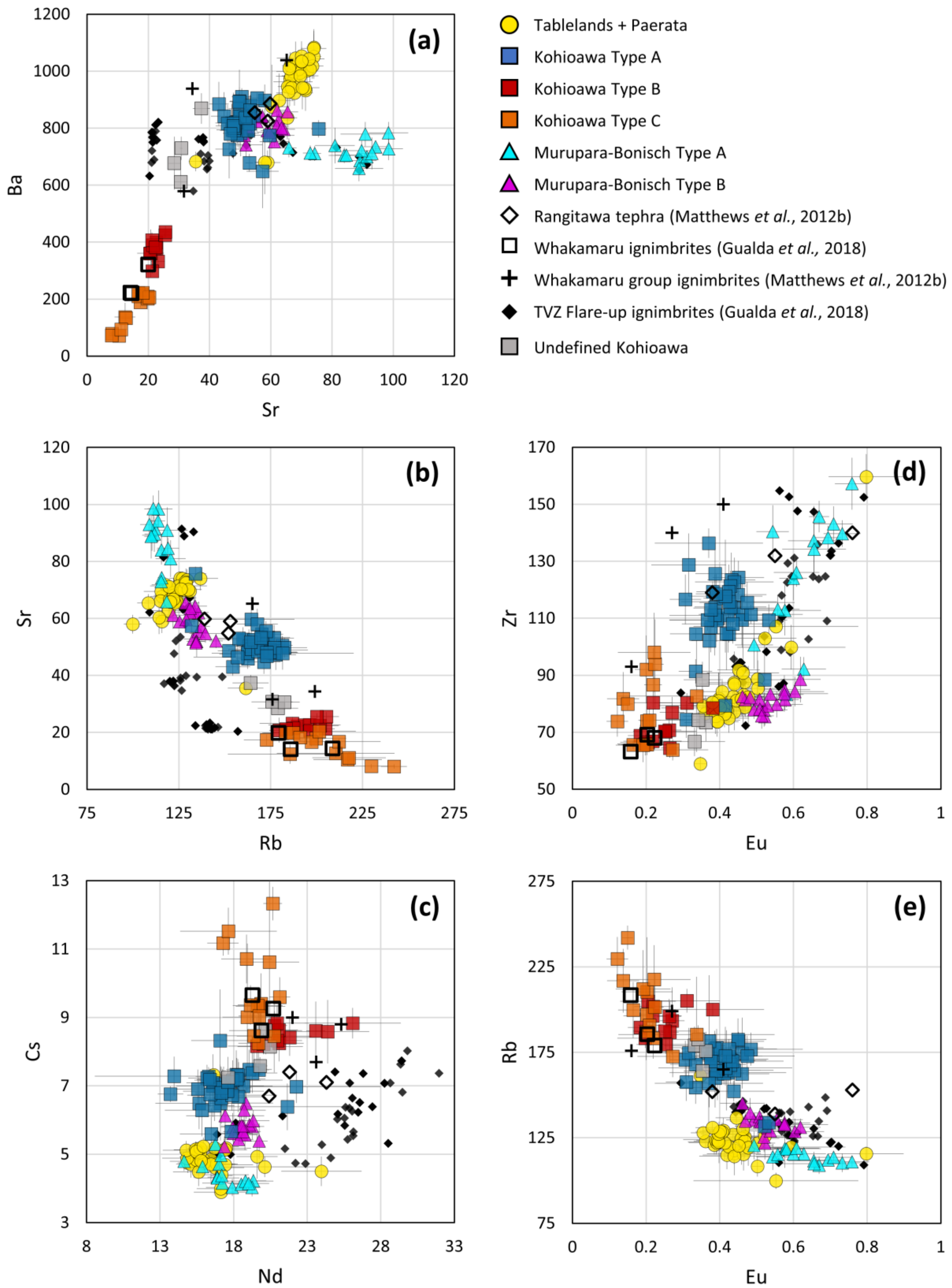

Figure 5 Trace-element compositions of glass from pumice clasts of the Kohioawa and Ōtarawairere sections in a) Ba vs. Sr; b) Sr vs. Rb; c) Cs vs. Nd; d) Zr vs. Eu; and

e) Rb vs. Eu space reported in ppm. We include literature data: 1) Rangitawa tephra data from Matthews *et al.* (2012b); 2) Whakamaru ignimbrite data from Gualda *et al.* (2018), represented by open black squares, and from Matthews *et al.* (2012b), represented by black crosses; 3) ignimbrite data from the TVZ from other ignimbrite flare-up eruptions from Gualda *et al.* (2018), represented by black diamonds. There are four undefined compositions from the Kohioawa tephras that do not fall into the three Kohioawa types, represented by gray squares. Different groups can be separated well using a combination of trace elements, particularly Ba and Sr.

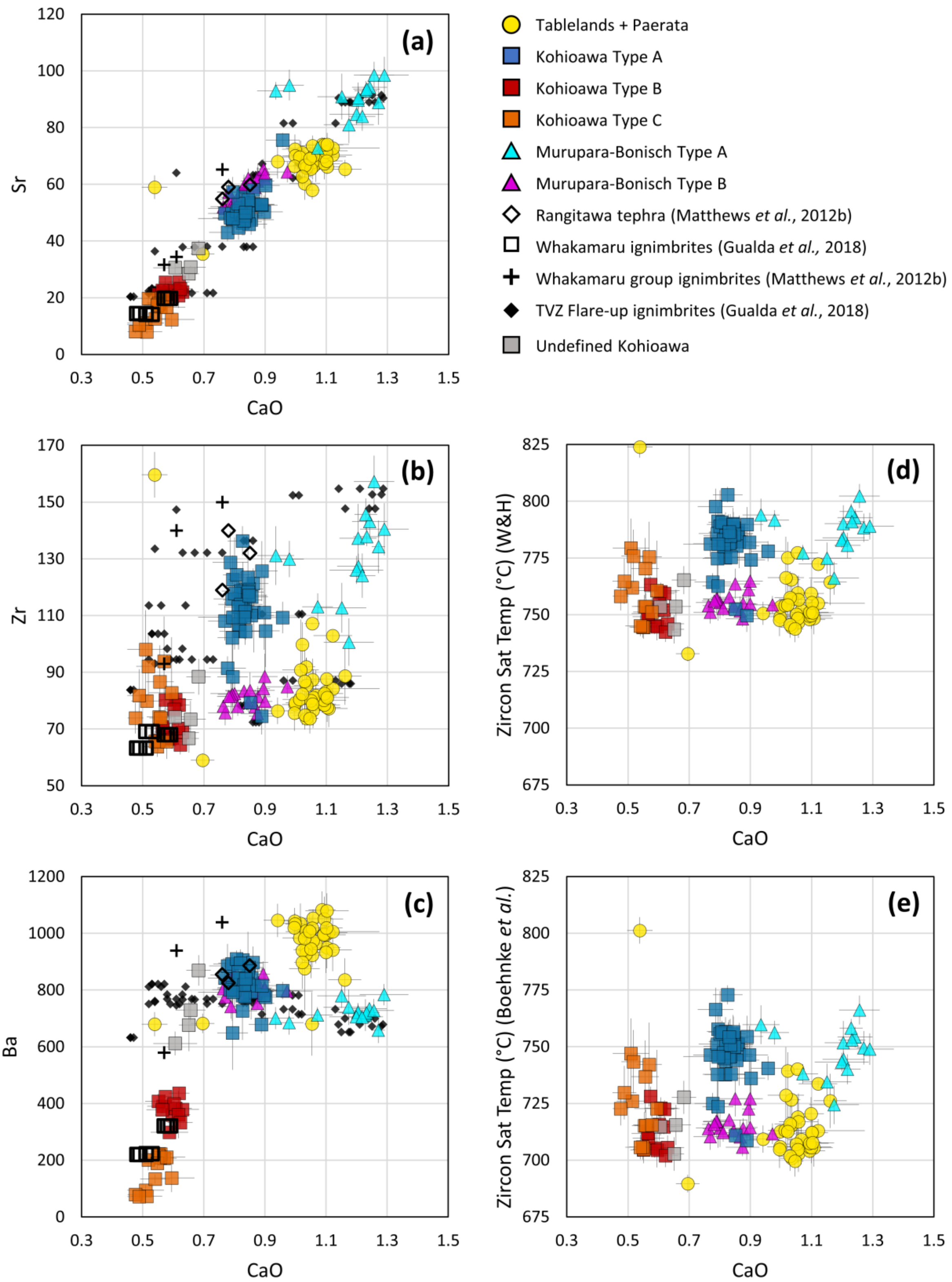

Figure 6 Select trace-element (ppm) and zircon-saturation temperatures (°C) vs. CaO (wt%) diagrams of glass from pumice clasts of the Kohioawa and Ōtarawairere

sections. Zircon-saturation temperatures are calculated using the Watson and Harrison (1983) calibration are labeled Zircon Sat Temp (W&H), panel d) and the Boehnke *et al*. (2013) calibration labeled Zircon Sat Temp (Boehnke *et al.*), panel e). All magmas are assumed to be zircon saturated, so temperatures represent pre-eruptive magmatic temperatures. Error bars (gray bars) are shown at the 1-sigma level for major and trace elements. The combination of CaO, Sr, and Ba leads to clear separation between the different magma types identified in this work. Zircon saturation temperatures are similar to each other, with Kohioawa type A and Murupara-Bonisch type A showing somewhat higher temperatures than the other units.

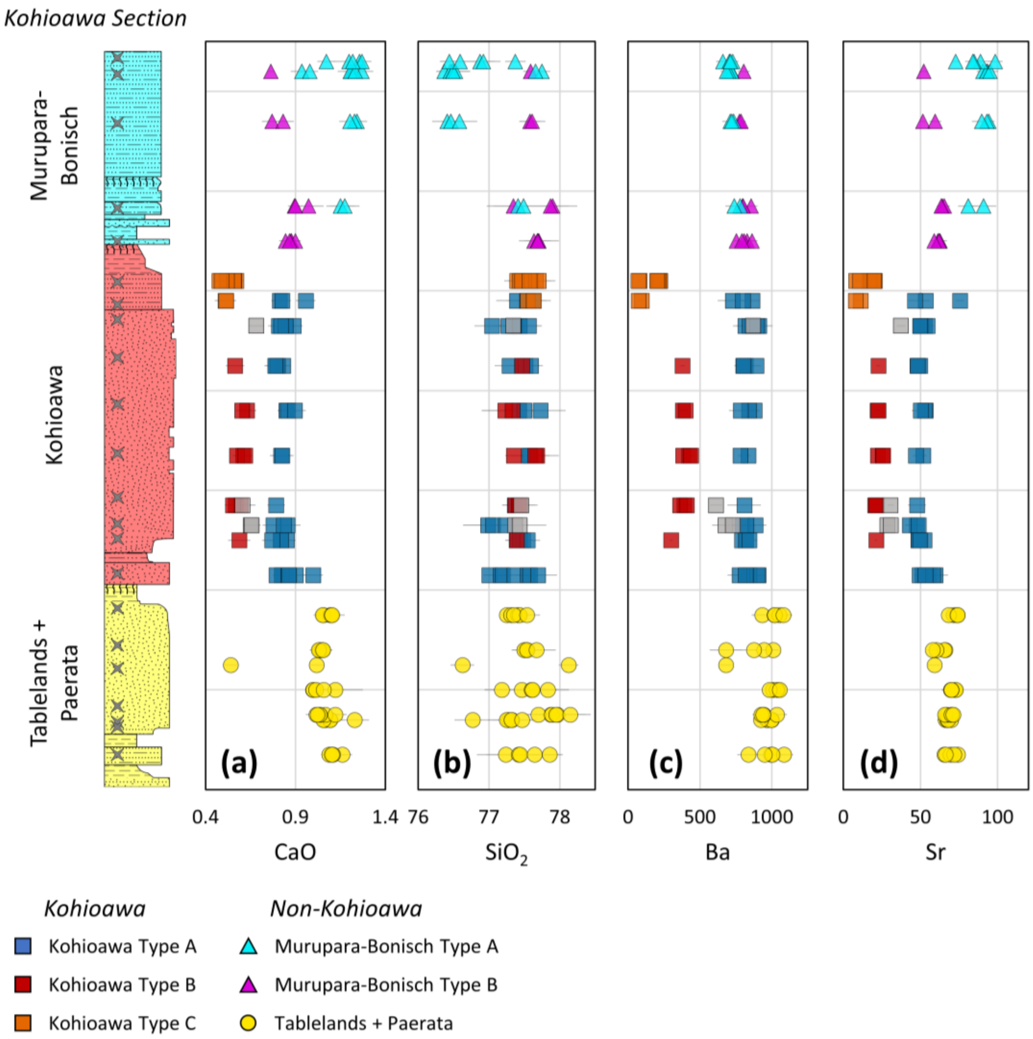

Figure 7 Major and trace-element compositions of glass from pumice clasts of the Kohioawa section as a function of height in the section. The yellow basal unit comprises the Tablelands and Paerata unit; the red middle unit is Kohioawa unit; the top light-blue unit is the Murupara-Bonisch unit. Elements shown are a) CaO (wt%); b) SiO_2 (wt%); c) Ba (ppm); and d) Sr (ppm). Note that Kohioawa type A is the only type present in the lower subunit of the Kohioawa unit, while Kohioawa type C is the only type present in the upper subunit of the Kohioawa unit. Also note the sharp compositional transitions from Tablelands and Paerata to Kohioawa to Murupara-Bonisch units. Symbology as in Figure 4-6.

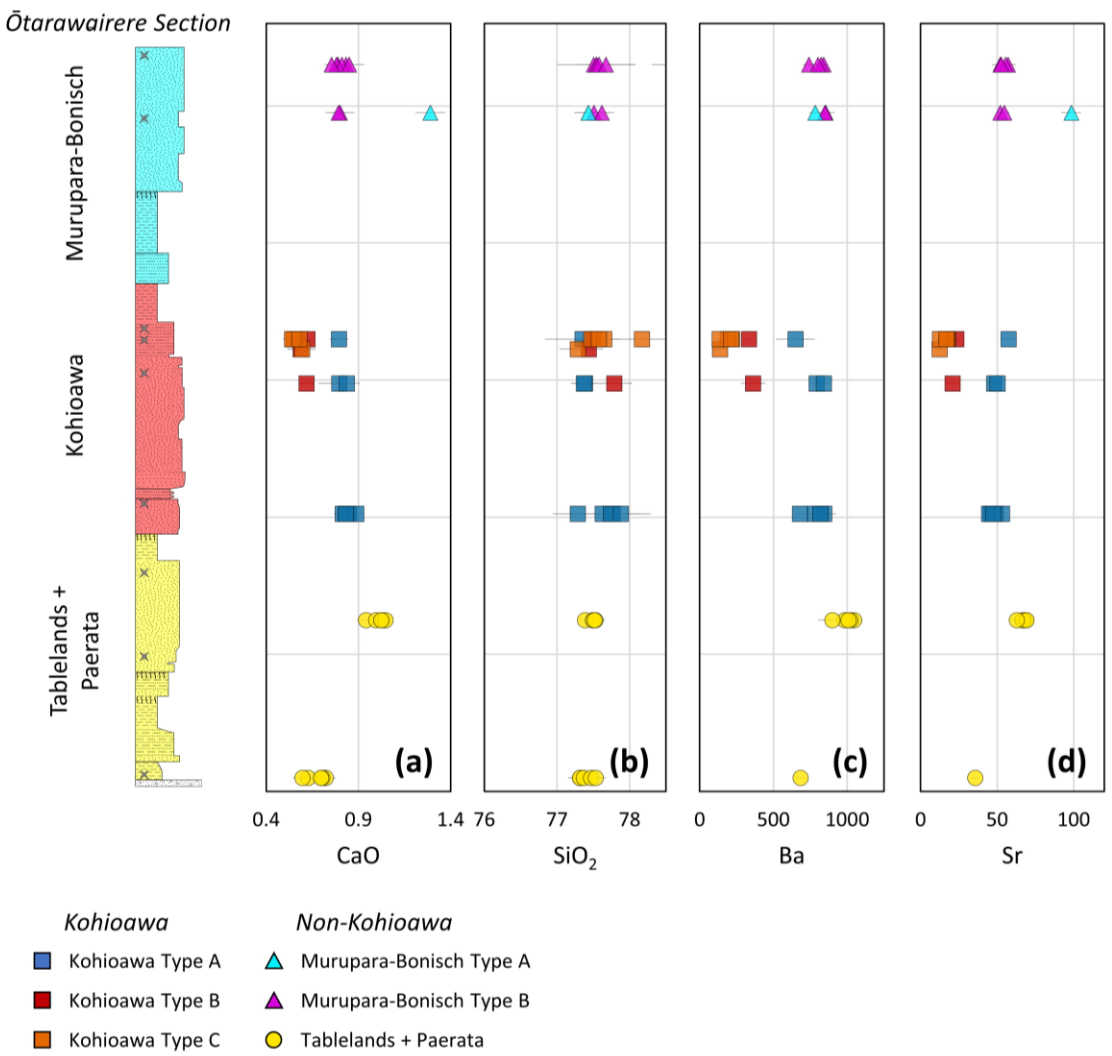

Figure 8 Major and trace-element compositions of glass from clasts of the Ōtarawairere section as a function of height in the section. The yellow basal unit comprises the Tablelands and Paerata unit; the red middle unit is Kohioawa unit; the top light-blue unit is the Murupara-Bonisch unit. Elements shown are a) CaO (wt%); b) SiO_2 (wt%); c) Ba (ppm); and d) Sr (ppm). The number of samples from the Ōtarawairere section is much smaller than from the Kohioawa section, but the general observations are consistent between the two sections with the exception that the uppermost sampled horizon in the Kohioawa unit shows Kohioawa types A, B, and C are present in this horizon. Symbology as in Figure 4-6.

Geothermometry

We calculate zircon saturation temperatures for all clasts using the calibrations of Watson and Harrison (1983) and Boehnke *et al*. (2013). The temperature for each clast is included in the supplementary data. The uncertainties of individual clasts are calculated using the uncertainties of Zr; uncertainties introduced by the major-element compositions are minimal, as the M values (calculated using the major-element compositions) range from 0.836-1.34, with an average of 1.03 and a standard deviation of 0.081 and have a small impact on the calculation. Uncertainties for the average zircon saturation temperature per type are calculated as the standard deviation of zircon saturation temperatures for the given type. The average and standard deviation zircon saturation temperatures for each type are (Figures 6c and 6e): 757 ± 15 °C for Tablelands B, Tablelands D, and Paerata (using the Watson and Harrison (1983) calibration; 716 ± 19 °C using the Boehnke *et al*. (2013) calibration); 782 ± 10 °C (746 ± 13 °C) for Kohioawa type A; 752 ± 7 °C (713 ± 9 °C) for Kohioawa type B; 760 ± 12 °C (724 ± 14 °C) for Kohioawa type C; 787 ± 12 °C (748 ± 11 °C) for Murupara-Bonisch type A; and 756 ± 4 °C (716 ± 6 °C) for Murupara-Bonisch type B.

Geobarometry

We use rhyolite-MELTS geobarometry to determine the storage conditions of the pre-eruptive magmas (Figures 9-10 and Figure 12, see discussion). Of the 153 clast compositions, 121 compositions (79%) yield storage pressures (supplementary data). Individual pressure calculations are reported to the nearest 1 MPa (e.g., 122 MPa), and ranges of pressures are rounded to the nearest 5 MPa (e.g., 100-125 MPa).

All storage pressures are shallow, upper crustal pressures of 50-255 MPa, with 90% of the data in the 70-235 MPa range, and with clasts of each compositional type exhibiting a narrower range of pressures (Figures 9-10 and Figure 12, see discussion). The Tablelands B, Tablelands D, and Paerata type shows a slightly larger pressure range, with 75% of the pressures in the 75-155 MPa range. The Kohioawa types all have shallow pressures, with 75% of the pressure ranges of 75-120 MPa for type A, 80-115 MPa for type B, and 60-135 MPa for type C. For types C, all three pressures ≤ 75 MPa are qtz-1feld pressures. The Murupara-Bonisch type B shows shallower pressures and Murupara-Bonisch type A shows deeper pressures. For Murupara-Bonisch type B, 75% of the pressures are in the 75-140 MPa range, contrasted with Murupara-Bonisch type A, where 75% of the pressures are within 110-245 MPa. Uncertainties estimated by Pitcher *et al.* (2021) show that the qtz-2feld pressures have a 1-sigma standard deviation of 24 MPa and the qtz-1feld pressures have a 1-sigma standard deviation of 38 MPa. Uncertainties obtained via a Montecarlo error analysis on a glass composition from a pumice clast from the Whakamaru ignimbrite (whose composition was obtained using the same methods as this work) exhibit a qtz-2feld 1-sigma standard deviation of 13 MPa with several qtz-1feld results showing <22 MPa 1-sigma standard deviation (Smithies *et al.*, 2023). In all figures that contain geobarometry results, we plot the more conservative uncertainties of Pitcher *et al.* (2021).

Most clast compositions that produced a storage pressure yield pressures with the mineral assemblage qtz-1feld (101/121 successful pressure calculations). With the exception of one Paerata clast (no sanidine observed in the horizon), the Kohioawa types B and C (all from sanidine-bearing horizons) are the only types to yield storage pressures with a qtz-2feld assemblage (19 compositions). The presence of the qtz-2feld assemblage indicates that these are the only compositional types with glass compositions consistent with sanidine saturation.

A total of 19/26 of the Kohioawa types B and C clasts produced qtz-2feld pressures, while the other 7/26 Kohioawa types B and C clasts produced qtz-1feld pressures. Of the 7, two (2/7) are shallow (50 MPa) pressures and an additional 2/7 are from the "undefined" Kohioawa clasts, indicating that the vast majority of the pressures from this group yields qtz-2feld pressures.

There are 31 compositions for which the quartz and plagioclase saturation surfaces become coincident at ≤ 100 MPa (see Methods). There were 7 compositions from the Tablelands B, Tablelands D, and Paerata type, 15 from the Kohioawa type A, 1 from Kohioawa type B, 3 from Kohioawa type C, 0 from Murupara-Bonisch type A, and 5 from Murupara-Bonisch type B. Of these, in instances when a storage pressure was calculated, the mean pressure calculated was 53 MPa, and the corrected mean pressure estimated is 81 MPa (pressures are documented as 50, 75, or 100 MPa depending on the point at which the saturation curves begin to become coincident within 5 °C). The original and updated calculations indicate that these are from compositions that exhibited predominantly shallow pressures.

There are several pressure trends through time that become apparent (Figure 9). There are consistent shallow storage pressures until the second horizon in the Murupara-Bonisch unit, where there are deeper storage pressures of ~200-275 MPa. There are several horizons that exhibit clasts with low pressures (~50 MPa), particularly within the Kohioawa horizons.

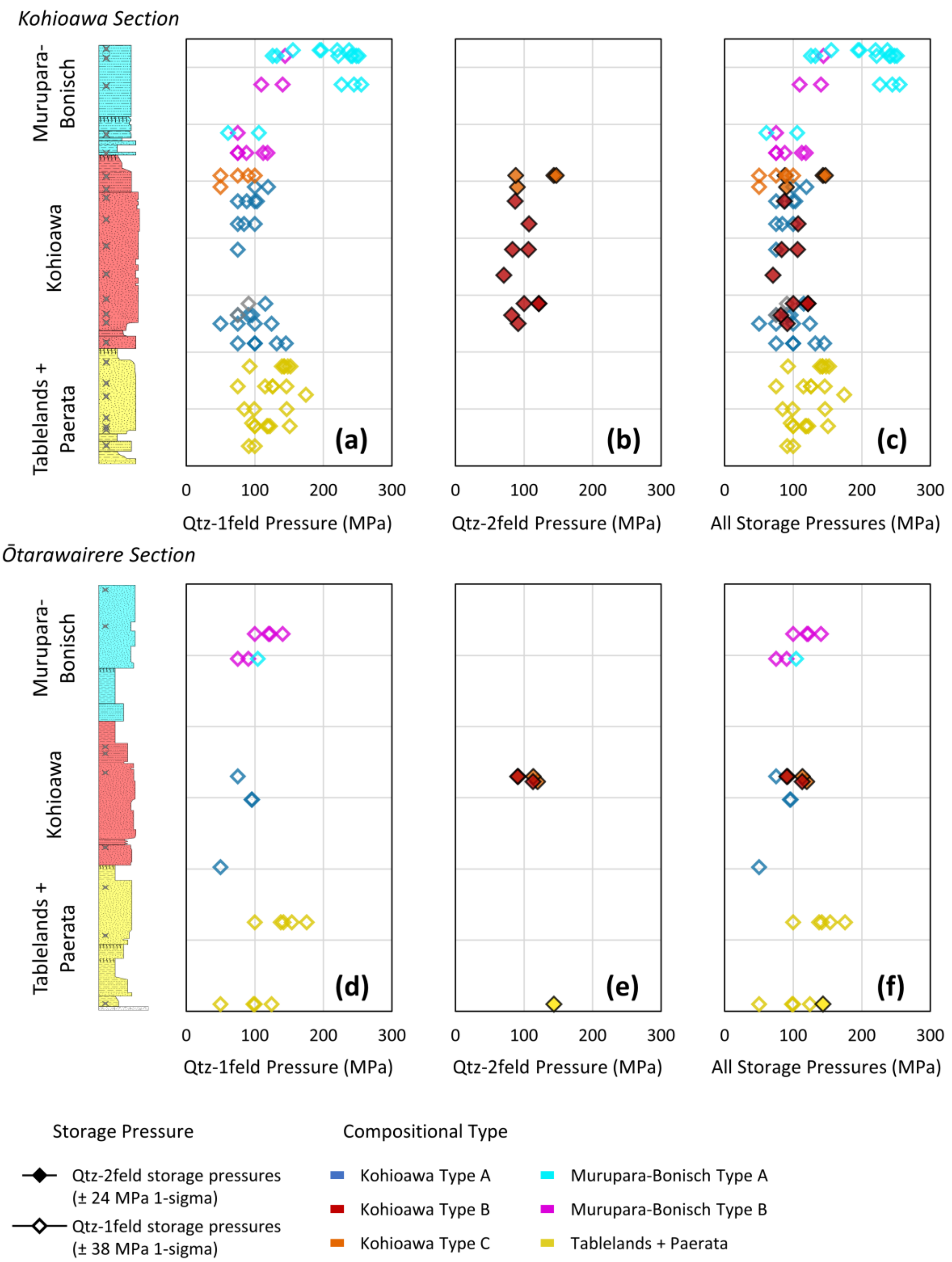

769

770 **Figure 9** Rhyolite-MELTS storage pressures for glass from pumice clasts of the

771 Kohioawa (top panels) and Ōtarawairere (bottom panels) sections as a function of

772 height through the sections. All pressures are reported in MPa. Left panels (a and d)

show pre-eruptive storage pressures for clasts that returned quartz+plagioclase (qtz-1feld) pressures. Middle panels (b and e) show pre-eruptive storage pressures for clasts that returned quartz+plagioclase+sanidine (qtz-2feld) pressures. Right panels (c and f) show all pressures, with filled diamonds representing qtz-2feld solutions and open diamonds representing quartz-1feld solutions. The Tablelands and Paerata unit yield exclusively qtz-1feld solutions, with resulting pressures similar to those seen in Kohioawa units; note the similarity in pressures between qtz-1feld and qtz-2feld solutions for the Kohioawa unit; Murupara-Bonisch unit only yield qtz-1feld solutions, with significantly deeper magma storage conditions for Murupara-Bonisch type A.

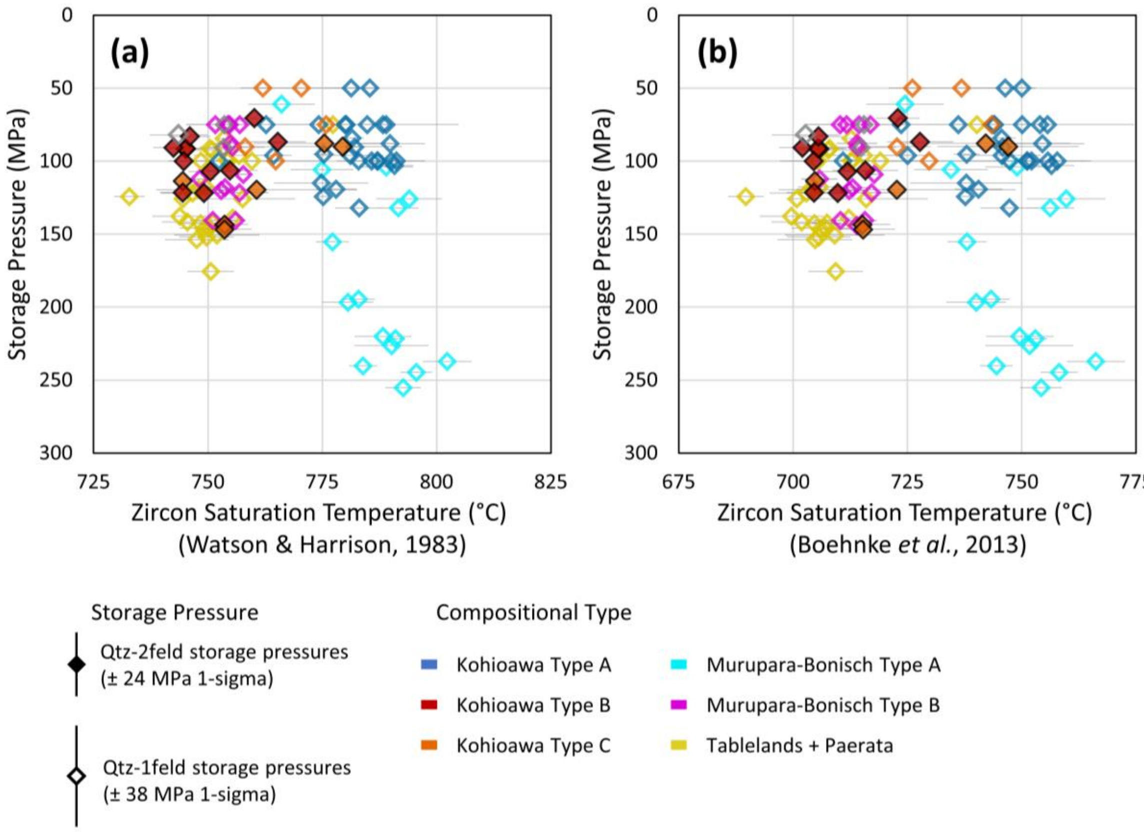

Figure 10 Binary diagrams comparing rhyolite-MELTS storage pressure calculations and zircon-saturation temperatures for average glass compositions from pumice clasts

of the Kohioawa and Ōtarawairere sections. Temperatures are calculated using (a) the Watson & Harrison (1983) calibration and (b) the Boehnke *et al.* (2013) calibration. Note that Kohioawa type A magmas have storage temperatures ~20 °C higher than Kohioawa types B and C magmas, despite similar storage pressures. Symbology as in Figure 9.

DISCUSSION

Correlating the Kohioawa tephra with the Whakamaru group ignimbrites

Previous studies have proposed a correlation between the Kohioawa tephra and the Whakamaru group ignimbrites (Manning, 1995, 1996), and likewise other studies have linked the Rangitawa tephra to the Whakamaru group ignimbrites (Froggatt *et al.*, 1986; Kohn *et al.*, 1992; Pillans *et al.*, 1996; Matthews *et al.*, 2012b). Here, we provide further evidence from published TVZ glass compositions (Bégué *et al.*, 2014b; Gualda *et al.*, 2018) to confirm and strengthen this correlation (Figures 4, 5, 11). We demonstrate here that the Kohioawa tephras are correlative with the Whakamaru group ignimbrites and are distinct from other TVZ magmas (Deering *et al.*, 2010).

The Rangitawa tephra is described as a pyroclastic fall deposit that has a minimum volume estimate of ~400 km^3 DRE (Matthews *et al.*, 2012b) and has been previously correlated with the widespread Whakamaru group ignimbrites (Kohn *et al.*, 1992; Alloway *et al.*, 1993; Pillans *et al.*, 1996; Lowe *et al.*, 2001; Matthews *et al.*, 2012b, 2012a). Matthews *et al.* (2012b) emphasize that the distal Rangitawa tephra, which is interpreted to represent the Plinian eruption phase, is compositionally similar to Whakamaru type A pumice from Brown *et al*. (1998), which is found in both the Whakamaru and Rangitaiki ignimbrites (Brown *et* *al.*, 1998; Matthews *et al.*, 2012b). Data from the Rangitawa tephra overlap with our Kohioawa type A glass in both major- and trace-element compositions (Figures 4-6, 11).

The Kohioawa tephras were partially correlated with the Whakamaru group ignimbrites by Manning (1996), who states that one of the glass populations was similar to the Rangitaiki ignimbrite but interprets the Kohioawa tephras to be from two coeval eruptions. Manning (1995, 1996) notes that the Kohioawa tephra deposits are the thickest in the region and estimates the age for the Kohioawa tephras to be ~350 ka using the reconstructed paleo sea level curve from O-isotopes, suggesting that the tephras were deposited just before the glacial maximum (delta-O^{18} stage 10), as evidenced by the presence of glacial loessic soil at the top of the Paerata unit just below the Kohioawa unit (Manning, 1995, 1996). However, there is no local sea level curve derived for the sequences and there are no independent numeric chronological control points.

By comparing our tephra data with published major- and trace-element glass data (Figure 11), we find that Kohioawa tephra glass compositions can be distinguished from other TVZ compositions. While Kohioawa type A is more similar to the other TVZ data, it does overlap with the Rangitawa tephra compositions (Matthews *et al.*, 2012b). In particular, Kohioawa types B and C overlap with the Whakamaru ignimbrite data (Bégué *et al.*, 2014b; Gualda *et al.*, 2018), which are compositionally distinct from all other TVZ magmas, likely due to being saturated in sanidine (Brown *et al.*, 1998; Gualda *et al.*, 2018).

In addition to the chemical comparisons, the field relations provide further evidence of the correlations. The Matahina ignimbrite overlies the Murupara-Bonisch tephra in the Kohioawa section, so the Kohioawa tephra must be older than the Matahina ignimbrite. Within the Kohioawa unit, the lack of a paleosol indicates that the tephras were deposited without significant (100s to 1000s a) time breaks, which is consistent with the overlapping Ar-Ar ages of the Whakamaru group ignimbrites (with the exception of the Paeroa Subgroup, as discussed above; see Downs et al., 2014). We thus concur with Manning (1995, 1996) that the Kohioawa tephra has the correct age and composition to be correlative with the Whakamaru group ignimbrites.

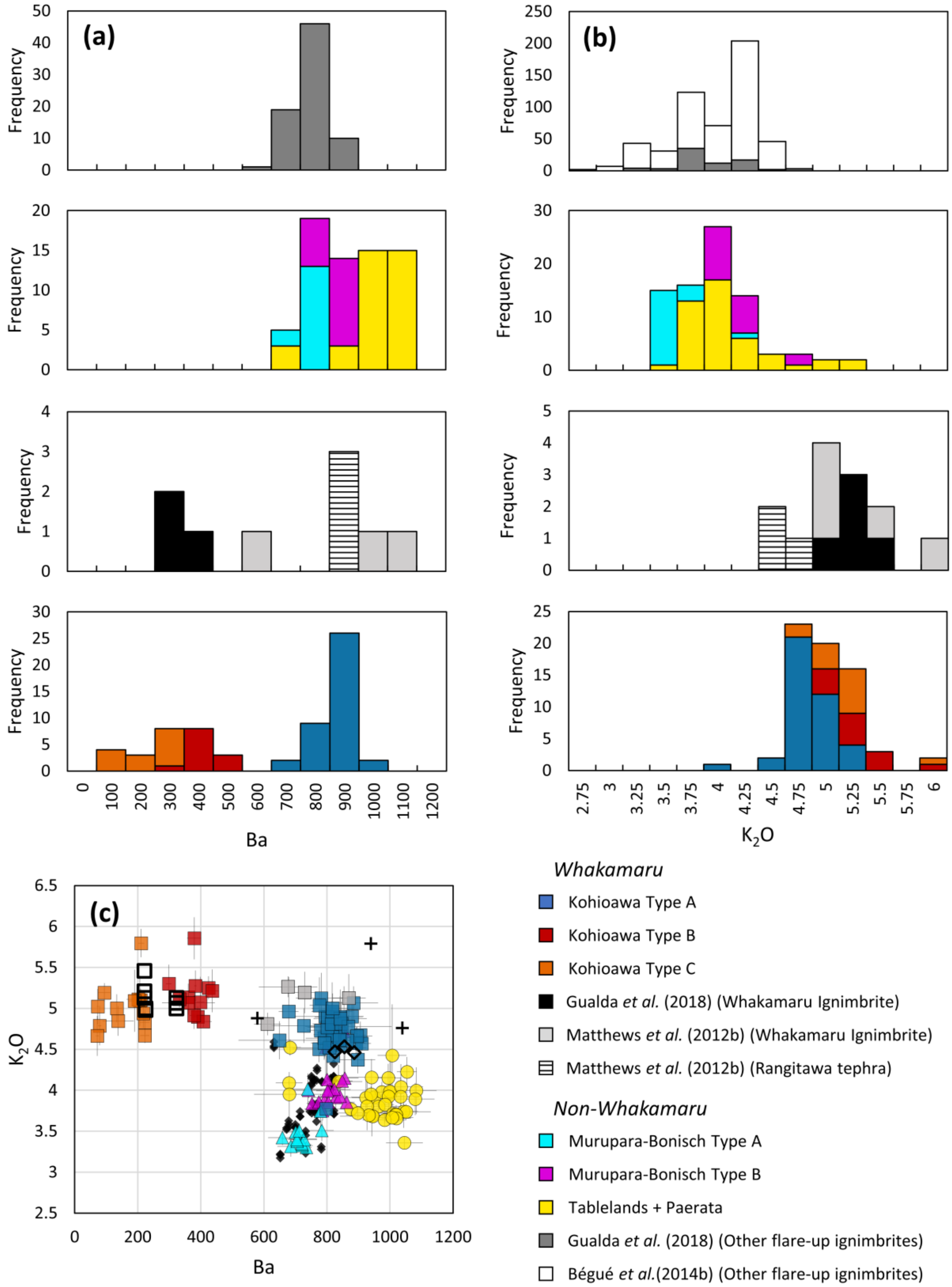

(a)
(b)
(c)
Frequency
Ba
K_2O
Whakamaru
Kohioawa Type A
Kohioawa Type B
Kohioawa Type C
Gualda et al. (2018) (Whakamaru Ignimbrite)
Matthews et al. (2012b) (Whakamaru Ignimbrite)
Matthews et al. (2012b) (Rangitawa tephra)
Non-Whakamaru
Murupara-Bonisch Type A
Murupara-Bonisch Type B
Tablelands + Paerata
Gualda et al. (2018) (Other flare-up ignimbrites)
Bégué et al.(2014b) (Other flare-up ignimbrites)

837

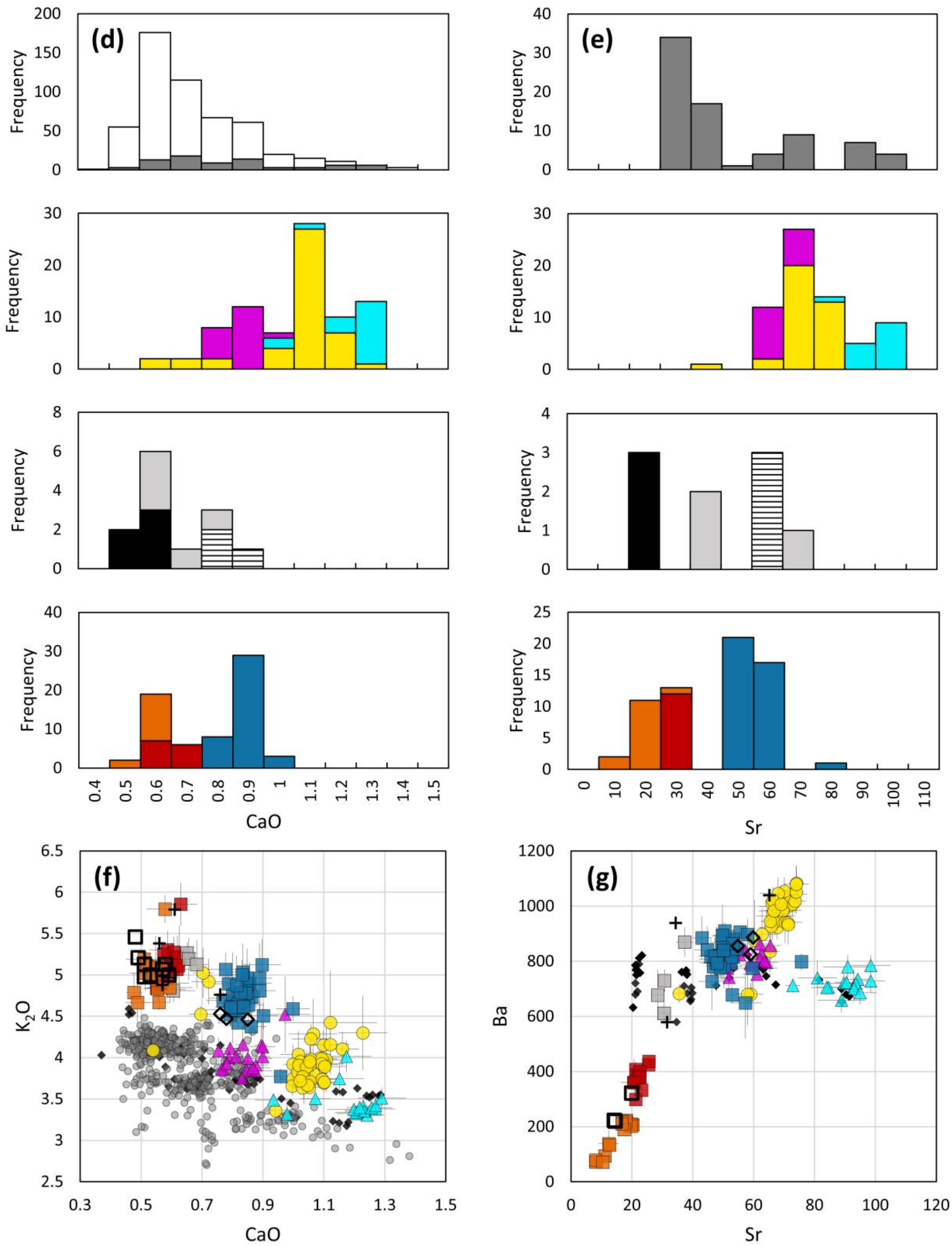

838

839 **Figure 11** Histograms (a, b, d, e) and binary diagrams (c, f, g) comparing data from

840 the Kohioawa unit (this work), Whakamaru ignimbrites (literature), other tephra units

from the studied tephras (this work), and other units from the Taupo Volcanic Zone (literature). Data from this work are shown in colors, while data from the literature are shown in grayscale. Symbology in binary diagrams as in Figures 4-6. Ba and K_2O distributions show that Whakamaru and Kohioawa compositions are distinct from other TVZ compositions and demonstrate that the Kohioawa unit corresponds to tephras correlative with the Whakamaru ignimbrites.

Magma types and different units

We interpret each clast as a small parcel of magma erupted but not fully fragmented during eruption. Glass compositions allow us to distinguish six compositional types in the clasts, which we interpret to represent six different types of magma that sourced the eruptions of the Tablelands B, Tablelands D, Paerata, Kohioawa, and Murupara-Bonisch eruptions. The lowermost units include a single type of magma that erupted to form the Tablelands B, Tablelands D, and Paerata tephras; the Kohioawa unit – which overlies the thickest paleosol – includes three distinct magma types that make up the Kohioawa tephras; and, finally, the topmost unit includes two distinct magma types that make up the Murupara-Bonisch tephras.

The glass from each of the three main units (Tablelands B & D/Paerata; Kohioawa; Murupara-Bonisch) has a unique compositional signature (Figures 4-6), consistent with the interpretation of Manning (1995) that these units were sourced from different volcanic centers. Our sampling of multiple horizons allows us to constrain the compositional boundaries, even where paleosols are not present.

The distinct paleosols within the sequences indicate significant time breaks between eruptions (Manning, 1995). It is difficult to constrain the duration of paleosol development but their thicknesses (e.g., ~40 cm at the top of the Paerata unit at the Ōtarawairere section and ~15 cm at the top of the Kohioawa unit at the Kohioawa section) suggest hiatuses of hundreds to thousands of years (Shoji *et al.*, 1994). After each paleosol, there is a change in glass composition that represents the onset of a new magma type.

The transitions in grain size within units (e.g., at 480-550 cm in the Kohioawa section, the uppermost Kohioawa package; Figures 1 and 2) indicate changes in eruption intensity for several of the eruptions (Houghton and Carey, 2015). There are two horizons at the Kohioawa section (one from 50-180 cm within the Paerata unit, the other 240-480 cm in the Kohioawa unit; Figure 2) that are much thicker and have relatively larger clasts than the other horizons, indicating more sustained, potentially Plinian-style eruptions.

Three different chemical compositions recognized in the Kohioawa unit and two additional types recognized in the Murupara-Bonisch unit indicate that multiple melt-dominated magma bodies contributed to these eruptions, similar to some other large eruptions e.g., the Mamaku and Ohakuri paired eruption (Bégué *et al.*, 2014a) and Kidnappers eruption (Cooper *et al.*, 2012), TVZ, New Zealand; Snake River Plain, USA (Ellis and Wolff, 2012; Swallow *et al.*, 2018); Bishop Tuff, Long Valley Caldera, USA (Gualda and Ghiorso, 2013); Tokachi and Tokachi-Mitsumata eruptions in central Hokkaido, Japan (Pitcher *et al.*, 2021). The lack of widespread evidence for mixing or mingling on the clast-scale suggests that the contemporaneous melt-dominated magma bodies were stored independently from one another and did not interact prior to eruption.

Magma types in the Kohioawa Sequence

The thickest unit studied, the Kohioawa tephra, shows distinct changes in the characteristics of the deposit through time. We identify three distinct packages within the Kohioawa unit. The lowermost package (~30-50 cm thick) is characterized by being massive, relatively grain-supported, with coarse-ash to fine-lapilli sized particles, and it is crystal-rich, which could suggest formation during a Plinian-style eruption based on grainsize characteristics (Houghton and Carey, 2015) and the geochemical correlation to the Rangitawa tephra. Our samples from this package (OK220707-1G at Kohioawa section and OK240707-1C at Ōtarawairere section) exhibit exclusively Kohioawa type A magma.

Above this package is the thickest package of the Kohioawa unit, which we propose could be a Plinian-style fall deposit due to the presence of fine lapilli and consistent grain size. Within this package, there are both Kohioawa type A and Kohioawa type B magma types in all horizons sampled, showing continued co-eruption of both magma types through most of the Kohioawa sequence (Figures 7 and 8).

At the top of the Kohioawa unit, the final package contains Kohioawa types A, B, and C, with Kohioawa type C exhibiting the most extreme compositions of the tephras (e.g., lowest CaO, Sr, and Ba) (Figure 7). This shift to include Kohioawa type C is correlated with a change in grainsize and sorting morphology from massive in the lower two packages to finely layered horizons in the uppermost Kohioawa package, which suggests that the tephras were deposited during pulsing eruptions, perhaps as co-ignimbrite fall deposits (Bonadonna *et al.*, 2015; Houghton and Carey, 2015).

The topmost package exhibits exclusively Kohioawa type C at the Kohioawa section, while the topmost horizon we sampled at the Ōtarawairere section exhibits all three Kohioawa magma types. This difference between sections could be attributed to sampling bias or could be that the top of the Ōtarawairere section has eroded and erased the uppermost horizons containing exclusively type C. The appearance of type C in only the uppermost package at both sections could be indicative of either: (1) the Kohioawa type C magma being segregated from the Kohioawa type B melt-dominated magma body as an independent melt-dominated magma body, and then further crystallizing, giving the glass a more extreme, depleted signature; or (2) that the final dregs of the Kohioawa type B melt-dominated magma body had a more fractionated geochemical signature of Kohioawa type C, which would indicate that there are compositional changes within the melt-dominated magma body in space, time, or both.

The compositional similarity between Kohioawa types B and C suggests that they are likely genetically related and possibly part of the same magmatic subsystem. In contrast, Kohioawa type A probably corresponds to an independent magmatic subsystem.

Kohioawa magmas and the Whakamaru group eruptions

Brown *et al*. (1998) describe four magma types in the Whakamaru group eruptions, based on whole-rock and glass analyses from single pumice clasts. Types A, B, and C observed by us in the Kohioawa tephras match types A, B, and C from Brown *et al*. (1998). We cannot effectively distinguish type D from type A using glass data alone – some of our type A compositions may indeed be type D. We note, however, that type D is much less abundant than type A in the dataset of Brown *et al*. (1998). As a result, we infer that only a small minority of our clasts could be type D.

The Kohioawa tephras provide a more complete record of the fall deposits formed by the Whakamaru eruptions than the Rangitawa tephras do, as the Rangitawa tephras only include type A magmas. The only horizon in the Kohioawa tephras that only include type A magmas is the basal subunit; we, thus, suggest that the widespread Rangitawa tephra is equivalent to the basal package of the Kohioawa tephra, which represents the initial eruption stage of the Whakamaru group. While this is corroborated by the geochemical observations of Matthews *et al.* (2012b), it contrasts with the interpretation that the Rangitawa tephra correlates to a later stage of the Whakamaru eruptions (Matthews *et al.*, 2012b).

It is interesting that the Kohioawa unit is the thickest and has the largest lapilli clasts within the tephras we studied, even though its source is inferred to be farther away (~90 km) than the source of the other units in the package (Ōkataina volcanic center, see Figure 1; Manning, 1995). This is consistent with the extreme size of the Whakamaru caldera-forming eruptions, i.e., a supereruption of more than 2000 km^3 DRE (Briggs, 1976a; Wilson *et al.*, 1986; Brown *et al.*, 1998; Matthews *et al.*, 2012b; Downs *et al.*, 2014).

Multiple eruptive pulses could reconcile previous work, which are contrasting in the interpretations of one versus multiple eruptions. Some previous studies describe the different ignimbrites as potentially different eruptions (Grindley, 1960; Martin, 1961; Briggs, 1976a, 1976b; Wilson *et al.*, 1986), while more recent work describes a single complex eruption episode for the Whakamaru group ignimbrites (with the Paeroa Subgroup as a second, younger eruption) (Brown *et al.*, 1998; Downs *et al.*, 2014). The lack of a paleosol within the Kohioawa tephras indicates that any break within the Whakamaru group eruptions would have to have been short, and likely not discernible via Ar-Ar ages (Downs *et al.*, 2014). However, the three distinct packages of the Kohioawa unit reveal three major eruptive phases of the Whakamaru group eruptions.

Kohioawa type A is the exclusive magma type present in the lowest Kohioawa package, which is consistent with the interpretation that sanidine was only present in later stages of the Whakamaru group ignimbrites (Ewart, 1965; Brown *et al.*, 1998). Kohioawa types A and B are present in approximately equal proportions in the middle package; and all three types are present in the uppermost package, where Kohioawa type C dominates, as indicated by the lower Sr and Ba signatures in the glass. The presence of sanidine-bearing Kohioawa type B from the second package through the top of the sequence indicates that only the first phase of the eruptions lacked sanidine. This shift to include Kohioawa type C indicates that the final phase of the eruptions included more evolved magmas than what is observed over the majority of the eruptions. Each clast has a distinct compositional signature, precluding any chemical mixing on the ash-to-lapilli-scale prior to eruption.

Storage conditions and architecture of the Whakamaru magma bodies

The tephra data show three distinct magma types that fed the Whakamaru group eruptions: Kohioawa types A, B, and C. The large negative Eu anomaly, low Ba content (Figure 5), and low CaO (Figures 4 and 6), among other attributes, illustrate that the similar Kohioawa types B and C magmas are the most distinct in this study. The presence of sanidine – as indicated by the mineralogy for the various horizons and also by rhyolite-MELTS calculations – suggests that Kohioawa types B and C are the only magmas saturated in sanidine. In contrast, the Kohioawa type A magma is mineralogically similar to pre-Kohioawa and post-Kohioawa magmas, although it is still compositionally distinct from the other magma types, as indicated by the glass compositions (Figures 4-6, 11).

All three Kohioawa magma types are stored at the same shallow pre-eruptive storage pressures (50-150 MPa), indicating that the magmas coexist at the same pre-eruptive storage depth within the crust (Figure 12). There are certain horizons that show slightly shallower or slightly deeper storage pressures (Figure 10), but all storage pressures are within 50-150 MPa. The Kohioawa type B and type C magmas likely have a tightly constrained storage pressure, as most of the pressures are constrained to ~70-150 MPa and these storage pressures are predominantly qtz-2feld, which have smaller uncertainties of ± 24 MPa 1-sigma (Pitcher *et al.*, 2021), whereas the Kohioawa type A magma has a wider storage range of 50-150 MPa.

Our storage pressures are in contrast with the model of Brown *et al*. (1998), which envisioned a single, stratified magma body, with three main types of magma that are connected (Whakamaru types A, B, and C), forming a zoned magma body with the most fractionated magma at the top of the magma body, with crystal fractionation playing a dominant role in differentiating magma types. As both Kohioawa types A and B yield overlapping storage pressures and both erupted continuously throughout the eruption, our data are inconsistent with the presence of a single zoned magma body. Instead, we conclude that there existed at least two melt-dominated magma bodies, which were laterally juxtaposed, existing at the same crustal level. One melt-dominated magma body consistently erupted Kohioawa type A, while another melt-dominated magma body erupted Kohioawa type B. The Kohioawa type C magma only erupted in the final stages of the eruption, and it is likely geochemically linked to Kohioawa type B, due to the compositional similarity.

Further evidence for the presence of multiple melt-dominated magma bodies is provided by zircon saturation temperatures. The temperatures calculated for Kohioawa type A are systematically hotter than those calculated for Kohioawa types B and C (Figure 10). The cooler temperatures of Kohioawa types B and C are very similar to both the Tablelands B, Tablelands D, and Paerata type and the Murupara-Bonisch type B temperatures. While we have not documented zircon in the clasts, likely due to the small sizes of the ash-lapilli clasts and likely sparse grains of zircon, there is compositional evidence for its presence. Previous studies have documented the presence of zircon in type A pumice clasts from the Whakamaru group ignimbrites (Brown, 1994; Matthews, 2011). As all Kohioawa magmas are high-silica rhyolites, Zr is lowest in the most fractionated glasses (Figure 4). Zr/Hf is fairly low in type

A, very low in type B, and extremely low in type C, it is therefore likely that they are saturated in zircon, indicating that the temperatures record the storage conditions of the magmas. These potential uncertainties notwithstanding, the Zr concentrations we document further demonstrate that type A magmas are compositionally distinct from types B and C, reinforcing the idea that they represent different magma bodies.

The continuous deposition of both Kohioawa types A and B in the middle and uppermost Kohioawa packages indicates that both magma types erupted continuously, together throughout the eruption. They likely erupted from two separate, laterally juxtaposed melt-dominated magma bodies that were tapped during most of the eruptive event. The overlap in storage pressures and temperatures indicates that there is likely a segregated melt-dominated magma body that erupted Kohioawa type C independent from and laterally juxtaposed to Kohioawa type B in the final stages of the eruptions. While Kohioawa type C magma could be genetically related to Kohioawa type B magma (with type C being similar but more fractionated than type B), the processes linking the two magma types deserves further study.

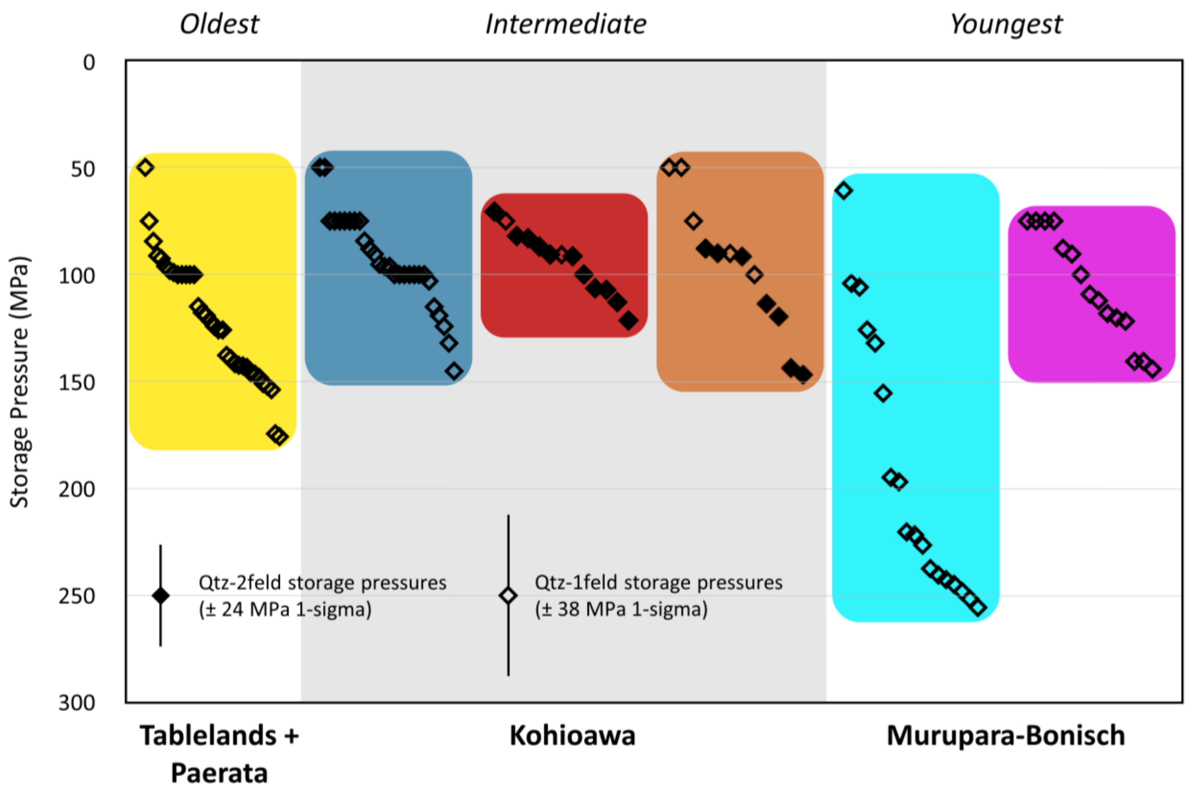

Figure 12 Rank order diagram of rhyolite-MELTS storage pressures with superimposed schematic of distribution of magma bodies as a function of depth. Crosses indicate qtz-1feld pressure results, and filled circles represent qtz-2feld pressure results. Configuration inferred for the Tablelands and Paerata unit (oldest in the sequence) appears on the left; configuration for the Kohioawa unit appear in the middle portion of the figure; configuration for the Murupara-Bonisch unit (youngest in the sequence) appear on the right. There could be multiple magma bodies based on the storage pressures for a given magma type, although we draw only one magma body per magma type due to the 1-sigma uncertainty from the pressure results. There is one magma type that erupted the Tablelands and Paerata tephras, three magma types that contributed to the Kohioawa eruptions (which are correlative with the Whakamaru eruptions), and two magma types that erupted during the Murupara-

Bonisch eruptions. The Whakamaru eruptions commenced with the Kohioawa type-A magma and erupted both types A (blue) and B (red) for most of the eruptions, and erupted types A, B, and C (orange) in the final stages of the Whakamaru eruptions.

Whakamaru group eruptions in the context of the TVZ Ignimbrite Flare-Up

Tephra compositions and calculated storage pressures show that each magma type displays a narrow compositional range, and they erupt from a narrow pressure range (Figure 12). Most units show storage pressures of 75-150 MPa, indicating a consistent and narrow storage zone within the shallow crust that is repeated through the eruptions. Given that this pressure interval prevails over most of the eruptions studied here, it seems likely that it reveals a structural or tectonic control on the storage level of these magmas. This is consistent with what can be inferred from the results of Bégué *et al*. (2014b) for the central TVZ as a whole (see also Cooper *et al.*, 2012; Allan *et al.*, 2013).

The Murupara-Bonisch unit is the only one that has a distinct pressure change through the eruptions, as the Murupara-Bonisch type A magmas erupt from much deeper storage pressures of ~105-250 MPa (Figures 9 and 12). This deeper signature is consistent with the deeper storage pressures inferred for the magmas in the Chimpanzee and Pokai eruptions (Gualda *et al.*, 2018; Smithies *et al.*, 2023) – the caldera-forming eruptions that follow the Whakamaru group eruptions during this TVZ flare-up. The deeper storage pressures after the Whakamaru group eruptions show that there must have been a reorganization in the crust after the Whakamaru group eruptions expelled such a large volume of magma (see Gravley *et al.*, 2016).

CONCLUSIONS

In this work, we use a combination of field and laboratory characterization of two tephra sequences in the Bay of Plenty, Aotearoa New Zealand, focusing on glass geochemistry and determination of crystallization conditions using rhyolite-MELTS geobarometry and zircon-saturation geothermometry.

The tephra units that precede the Kohioawa tephras represent the smaller Tablelands and Paerata eruptions that likely erupted from the Ōkataina volcanic center. These units are compositionally similar and have shallow storage pressures (90% of pressures 50-135 MPa). These units represent magmas that are consistent with what is generally observed in the central TVZ (Bégué *et al.*, 2014b).

We leverage the unique mineralogy and glass compositions of Whakamaru magmas to demonstrate that the Kohioawa unit is correlative with the Whakamaru ignimbrites and the Rangitawa tephra, consistent with previous studies (Froggatt *et al.*, 1986; Kohn *et al.*, 1992; Pillans *et al.*, 1996; Brown *et al.*, 1998; Matthews *et al.*, 2012b). Combining volcanological information from the tephras with petrological inferences using glass compositions, we provide new information on the eruptive history and the architecture of the Whakamaru magmatic system.

During the initial stages of the Whakamaru group eruptions, only type A magmas erupted, suggesting that the Rangitawa tephras are correlative with this phase of the eruptions. Following this initial event, Kohioawa type A and B magmas erupt continuously through most of the Kohioawa sequence, suggesting the presence of at least two independent magma bodies (one sanidine-bearing, and one sanidine-absent) for most of the duration of the eruptions. The final stages of the Kohioawa unit include an additional third magma type (type C). This indicates a shift in the final stages of the eruptions to include a third magma body.

Our data do not support the model of Brown *et al*. (1998) of a single, vertically stratified magma body. Instead, our data suggest the presence of at least two (more likely three) laterally juxtaposed and chemically independent magma bodies. These bodies primarily appeared at pressures of 75-150 MPa (75% of data fall within this (depths of ~3-6 km, using an average crustal density of $2.7 * 10^3$ kg/m^3), but we find some evidence for accompanying shallower pressures of ~50 MPa (~2 km depth).

The succeeding Murupara-Bonisch tephras show a significant change in composition from R1 (cold, wet, oxidizing) to R1+R2 (cold, wet, oxidizing and hot, dry, reducing) magmas (Deering *et al.*, 2010), and they also show eruption of different magma types sourced from different storage levels. Even though they are sourced from the Ōkataina volcanic center, the dramatic shift in composition between Whakamaru-related magmas and Murupara-Bonisch magmas shows that the central TVZ magma systems went through a thorough reorganization following the Whakamaru event (Gravley *et al.*, 2016; Gualda *et al.*, 2018).

ACKNOWLEDGEMENTS

We would like to thank Ayla Pamukçu and Elizabeth Grant for help during field work in 2017. Thank you to Mark Ghiorso, Calvin Miller, Ayla Pamukçu, and Bradley Pitcher for advice on early drafts of the manuscript. This work was supported by the National Science Foundation [EAPSI-1714025 to L.J.H, EAR-1830122 to G.A.R.G.].

DATA AVAILABILITY STATEMENT

The quantitative data underlying this article are available in the article and in its online supplementary material. SEM BSE images of clasts will be shared on reasonable request to the corresponding author.

REFERENCES

Allan, A. S. R., Barker, S. J., Millet, M. A., Morgan, D. J., Rooyakkers, S. M., Schipper, C. I. & Wilson, C. J. N. (2017). A cascade of magmatic events during the assembly and eruption of a super-sized magma body. *Contributions to Mineralogy and Petrology* **172**, 49.

Allan, A. S. R., Morgan, D. J., Wilson, C. J. N. & Millet, M. A. (2013). From mush to eruption in centuries: Assembly of the super-sized Oruanui magma body. *Contributions to Mineralogy and Petrology* **166**, 143–164.

Alloway, B. V., Pillans, B. J., Sandhu, A. S. & Westgate, J. A. (1993). Revision of the marine chronology in the Wanganui Basin, New Zealand, based on the isothermal plateau fission-track dating of tephra horizons. *Sedimentary Geology* **82**, 299–310.

Bachmann, O. & Bergantz, G. W. (2004). On the origin of crystal-poor rhyolites: Extracted from batholithic crystal mushes. *Journal of Petrology* **45**, 1565–1582.

Bachmann, O. & Bergantz, G. W. (2008). The magma reservoirs that feed supereruptions. *Elements* **4**, 17–21.

Bailey, R. A. & Carr, R. G. (1994). Physical geology and eruptive history of the Matahina Ignimbrite, Taupo Volcanic Zone, North Island, New Zealand. *New Zealand Journal of Geology and Geophysics* **37**, 319–344.

Barboni, M., Annen, C. & Schoene, B. (2015). Evaluating the construction and evolution of upper crustal magma reservoirs with coupled U/Pb zircon geochronology and thermal modeling: A case study from the Mt. Capanne pluton (Elba, Italy). *Earth and Planetary Science Letters* **432**, 436–448.

Bégué, F., Deering, C. D., Gravley, D. M., Kennedy, B. M., Chambefort, I., Gualda, G. A. R. & Bachmann, O. (2014a). Extraction, storage and eruption of multiple isolated magma batches in the paired Mamaku and Ohakuri eruption, Taupo Volcanic Zone, New Zealand. *Journal of Petrology* **55**, 1653–1684.

Bégué, F., Gualda, G. A. R., Ghiorso, M. S., Pamukçu, A. S., Kennedy, B. M., Gravley, D. M., Deering, C. D. & Chambefort, I. (2014b). Phase-equilibrium geobarometers for silicic rocks based on rhyolite-MELTS. Part 2: application to Taupo Volcanic Zone rhyolites. *Contributions to Mineralogy and Petrology* **168**, 1–16.

Blundy, J. D. & Cashman, K. V. (2001). Ascent-driven crystallisation of dacite magmas at Mount St Helens, 1980-1986. *Contributions to Mineralogy and Petrology* **140**, 631–650.

Blundy, J. D. & Cashman, K. V. (2008). Petrologic reconstruction of magmatic system variables and processes. *Reviews in Mineralogy & Geochemistry* **69**, 179–239.

Boehnke, P., Watson, E. B., Trail, D., Harrison, T. M. & Schmitt, A. K. (2013). Zircon saturation re-revisited. *Chemical Geology* **351**, 324–334.

Bonadonna, C., Costa, A., Folch, A. & Koyaguchi, T. (2015). Chapter 33 - Tephra Dispersal and Sedimentation. In: Sigurdsson, H., *et al.* (eds.) *The Encyclopedia of Volcanoes (Second Edition).* Academic Press, 587–597.

Bonadonna, C. & Phillips, J. C. (2003). Sedimentation from strong volcanic plumes. *Journal of Geophysical Research: Solid Earth* **108**, B7, 2340.

Briggs, N. D. (1976a). Recognition and correlation of subdivisions within the Whakamaru ignimbrite, central North Island, New Zealand. *New Zealand Journal of Geology and Geophysics* **19**, 463–501.

Briggs, N. D. (1976b). Welding and crystallisation zonation in Whakamaru Ignimbrite, central North Island, New Zealand. *New Zealand Journal of Geology and Geophysics* **19**, 189–212.

Brown, R. J., Bonadonna, C. & Durant, A. J. (2012). A review of volcanic ash aggregation. *Physics and Chemistry of the Earth* **45–46**, 65–78.

Brown, S. J. A. (1994). Geology and geochemistry of the Whakamaru Group ignimbrites, and associated rhyolite domes, Taupo Volcanic Zone, New Zealand. Christchurch, University of Canterbury.

Brown, S. J. A. & Fletcher, I. R. (1999). SHRIMP U-Pb dating of the preeruption growth history of zircons from the 340 ka Whakamaru Ignimbrite, New Zealand: Evidence for >250 k.y. magma residence times. *Geology* **27**, 1035–1038.

Brown, S. J. A., Wilson, C. J. N., Cole, J. W. & Wooden, J. L. (1998). The Whakamaru group ignimbrites, Taupo Volcanic Zone, New Zealand: Evidence for reverse tapping of a zoned silicic magmatic system. *Journal of Volcanology and Geothermal Research* **84**, 1–37.

Cashman, K. V. & Giordano, G. (2014). Calderas and magma reservoirs. *Journal of Volcanology and Geothermal Research* **288**, 28–45.

Chambefort, I., Lewis, B., Wilson, C. J. N., Rae, A. J., Coutts, C., Bignall, G. & Ireland, T. R. (2014). Stratigraphy and structure of the Ngatamariki geothermal system from new zircon U–Pb geochronology: Implications for Taupo Volcanic Zone evolution. *Journal of Volcanology and Geothermal Research* **274**, 51–70.

Chamberlain, K. J., Wilson, C. J. N., Wallace, P. J. & Millet, M. A. (2015). Micro-analytical perspectives on the Bishop Tuff and its magma chamber. *Journal of Petrology* **56**, 605–640.

Charlier, B. L. A., Bachmann, O., Davidson, J. P., Dungan, M. A. & Morgan, D. J. (2007). The upper crustal evolution of a large silicic magma body: Evidence from crystal-scale Rb-Sr isotopic heterogeneities in the Fish Canyon magmatic system, Colorado. *Journal of Petrology* **48**, 1875-1894.

Cooper, G. F., Morgan, D. J. & Wilson, C. J. N. (2017). Rapid assembly and rejuvenation of a large silicic magmatic system: Insights from mineral diffusive profiles in the Kidnappers and Rocky Hill deposits, New Zealand. *Earth and Planetary Science Letters* **473**, 1–13.

Cooper, G. F., Wilson, C. J. N., Millet, M. A., Baker, J. A. & Smith, E. G. C. (2012). Systematic tapping of independent magma chambers during the 1Ma Kidnappers supereruption. *Earth and Planetary Science Letters* **313–314**, 23–33.

Cooper, K. M. (2017). What does a magma reservoir look like? The “crystal’s-eye” view. *Elements* **13**, 23–28.

Cooper, K. M. & Kent, A. J. R. (2014). Rapid remobilization of magmatic crystals kept in cold storage. *Nature* **506**, 480–483.

Costa, A., Folch, A., Macedonio, G., Giaccio, B., Isaia, R. & Smith, V. C. (2012). Quantifying volcanic ash dispersal and impact of the Campanian Ignimbrite super-eruption. *Geophysical Research Letters* **39**, L10310.

Deering, C. D., Bachmann, O. & Vogel, T. A. (2011). The Ammonia Tanks Tuff: Erupting a melt-rich rhyolite cap and its remobilized crystal cumulate. *Earth and Planetary Science Letters* **310**, 518–525.

Deering, C. D., Gravley, D. M., Vogel, T. A., Cole, J. W. & Leonard, G. S. (2010). Origins of cold-wet-oxidizing to hot-dry-reducing rhyolite magma cycles and distribution in the Taupo Volcanic Zone, New Zealand. *Contributions to Mineralogy and Petrology* **160**, 609–629.

Downs, D. T., Wilson, C. J. N., Cole, J. W., Rowland, J. V., Calvert, A. T., Leonard, G. S. & Keall, J. M. (2014). Age and eruptive center of the Paeroa Subgroup ignimbrites (Whakamaru Group) within the Taupo Volcanic Zone of New Zealand. *Bulletin of the Geological Society of America* **126**, 1131–1144.

Eastwood, A. A., Gravley, D. M., Wilson, C. J. N., Chambefort, I., Oze, C., Cole, J. W. & Ireland, T. R. (2013). U-Pb dating of subsurface pyroclastic deposits (Tahorakuri Formation) at Ngatamariki and Rotokawa Geothermal Fields. Proceedings, *35th New Zealand Geothermal Workshop*. Rotorua, New Zealand.

Ellis, B. S. & Wolff, J. A. (2012). Complex storage of rhyolite in the central Snake River Plain. *Journal of Volcanology and Geothermal Research* **211–212**, 1–11.

Ewart, A. (1965). Mineralogy and petrogenesis of the Whakamaru ignimbrite in the Maraetai area of the Taupo volcanic zone, New Zealand. *New Zealand Journal of Geology and Geophysics* **8**, 611–679.

Ewart, A. & Healy, J. (1966). Te Whaiti ignimbrites at Murupara. In: Thompson, B., Kermode, L. & Ewart, A. (eds) *New Zealand Volcanology, Central Volcanic Region*. New Zealand Department of Scientific and Industrial Research Information, 121–125.

Folch, A. & Felpeto, A. (2005). A coupled model for dispersal of tephra during sustained explosive eruptions. *Journal of Volcanology and Geothermal Research* **145**, 337–349.

Foley, M. L., Miller, C. F. & Gualda, G. A. R. (2020). Architecture of a super-sized magma chamber and remobilization of its basal cumulate (Peach Spring Tuff, USA). *Journal of Petrology* **61**, egaa020.

Froggatt, P., Nelson, C., Carter, L., Griggs, G. & Black, K. (1986). An exceptionally large late Quaternary eruption from New Zealand. *Nature* **319**, 578–582.

Gravley, D. M., Deering, C. D., Leonard, G. S. & Rowland, J. V. (2016). Ignimbrite flare-ups and their drivers: A New Zealand perspective. *Earth-Science Reviews* **162**, 65–82.

Gravley, D. M., Wilson, C. J. N., Leonard, G. S. & Cole, J. W. (2007). Double trouble: Paired ignimbrite eruptions and collateral subsidence in the Taupo Volcanic Zone, New Zealand. *Bulletin of the Geological Society of America* **119**, 18–30.

Griffin, W., Powell, W., Pearson, N. J. & O'Reilly, S. (2008). GLITTER: data reduction software for laser ablation ICP-MS. *Short Course Series* **40**, 308–311.

Grindley, G. (1960). Geological Map of New Zealand 1:250,000. *NZ Department of Scientific and Industrial Research*. Wellington, New Zealand.

Gualda, G. A. R. & Ghiorso, M. S. (2013). The Bishop Tuff giant magma body: an alternative to the Standard Model. *Contributions to Mineralogy and Petrology* **166**, 755–775.

Gualda, G. A. R. & Ghiorso, M. S. (2014). Phase-equilibrium geobarometers for silicic rocks based on rhyolite-MELTS. Part 1: Principles, procedures, and evaluation of the method. *Contributions to Mineralogy and Petrology* **168**, 1–17.

Gualda, G. A. R. & Ghiorso, M. S. (2015). MELTS-Excel: A Microsoft Excel-based MELTS interface for research and teaching of magma properties and evolution. *Geochemistry, Geophysics, Geosystems* **16**, 315–324.

Gualda, G. A. R., Ghiorso, M. S., Hurst, A. A., Allen, M. C. & Bradshaw, R. W. (2022). A complex patchwork of magma bodies that fed the Bishop Tuff supereruption (Long Valley Caldera, CA, United States): Evidence from matrix glass major and trace-element compositions. *Frontiers in Earth Science* **10**.

Gualda, G. A. R., Ghiorso, M. S., Lemons, R. v. & Carley, T. L. (2012a). Rhyolite-MELTS: a modified calibration of MELTS optimized for silica-rich, fluid-bearing magmatic systems. *Journal of Petrology* **53**, 875–890.

Gualda, G. A. R., Gravley, D. M., Conner, M., Hollmann, B., Pamukçu, A. S., Bégué, F., Ghiorso, M. S. & Deering, C. D. (2018). Climbing the crustal ladder: Magma storage-depth evolution during a volcanic flare-up. *Science Advances* **4**, eaap7567.

Gualda, G. A. R., Pamukçu, A. S., Ghiorso, M. S., Anderson Jr, A. T., Sutton, S. R., Rivers, M. L. & Houlie, N. (2012b). Timescales of quartz crystallization and the longevity of the Bishop giant magma body. *PLoS ONE* **7**, e37492.

Gualda, G. A. R. & Sutton, S. R. (2016). The year leading to a supereruption. *PLoS ONE* **11**, 1–18.

Harmon, L. J., Cowlyn, J., Gualda, G. A. R. & Ghiorso, M. S. (2018). Phase-equilibrium geobarometers for silicic rocks based on rhyolite-MELTS. Part 4: Plagioclase, orthopyroxene, clinopyroxene, glass geobarometer, and application to Mt. Ruapehu, New Zealand. *Contributions to Mineralogy and Petrology* **173**, 7.

Healy, J., Schofield, J. & Thompson, B. (1964). *Sheet 5, Rotorua. Geological Map of New Zealand 1:250,000*. Wellington.

Hildreth, W. (1979). The Bishop Tuff: Evidence for the origin of compositional zonation in silicic magma chambers. *Geological Society of America* **180**, 43-75.

Hildreth, W. & Wilson, C. J. N. (2007). Compositional zoning of the Bishop Tuff. *Journal of Petrology* **48**, 951–999.

Holt, K. A., Wallace, R. C., Neall, V. E., Kohn, B. P. & Lowe, D. J. (2010). Quaternary tephra marker beds and their potential for palaeoenvironmental reconstruction on Chatham Island, east of New Zealand, southwest Pacific Ocean. *Journal of Quaternary Science* **25**, 1169–1178.

Houghton, B. & Carey, R. J. (2015). Chapter 34 - Pyroclastic Fall Deposits. In: Sigurdsson, H. (ed.) *The Encyclopedia of Volcanoes (Second Edition)*. Amsterdam: Elsevier, 599–616.

Houghton, B. F., Wilson, C. J. N., McWilliams, M. O., Lanphere, M. A., Weaver, S. D., Briggs, R. M. & Pringle, M. S. (1995). Chronology and dynamics of a large silicic magmatic system: Central Taupo Volcanic Zone, New Zealand. *Geology* **23**, 13–16.

Kaiser, J. F., de Silva, S., Schmitt, A. K., Economos, R. & Sunagua, M. (2017). Million-year melt–presence in monotonous intermediate magma for a volcanic–plutonic assemblage in the Central Andes: Contrasting histories of crystal-rich and crystal-poor super-sized silicic magmas. *Earth and Planetary Science Letters* **457**, 73–86.

Kohn, B. P., Pillans, B. & Mcglone, M. S. (1992). Zircon fission track age for middle Pleistocene Rangitawa Tephra, New Zealand: stratigraphic and paleoclimatic significance. *Palaeogeography, Palaeoclimatology, Palaeoecology* **95**, 73–94.

Leonard, G. S., Begg, J. G. & Wilson, C. J. N. (2010). Geology of the Rotorua area. Lower Hutt, New Zealand: GNS Science.

Lowe, D. J., Tippett, J. M., Kamp, P. J. J., Liddell, I. J., Briggs, R. M. & Horrocks, J. L. (2001). Ages on weathered Plio-Pleistocene tephra sequences, western North Island, New Zealand. In: Juvigné, E. T. & Raynal, J-P. (eds) "Tephras: Chronology, Archaeology", CDERAD éditeur, Goudet. *Les Dossiers de l'Archéo-Logis* **1**, 45-60.

Manning, D. A. (1995). Late Pleistocene tephrostratigraphy of the eastern Bay of Plenty region, New Zealand. Wellington, Victoria University.

Manning, D. A. (1996). Middle-late Pleistocene tephrastratigraphy of the eastern Bay of Plenty, New Zealand. *Quaternary International* **34–36**, 3–12.

Martin, R. C. (1961). Stratigraphy and structural outline of the Taupo Volcanic Zone. *New Zealand Journal of Geology and Geophysics* **4**, 449–478.

Martin, R. C. (1965). Lithology and eruptive history of the Whakamaru ignimbrites in the Maraetai area of the Taupo volcanic zone, New Zealand. *New Zealand Journal of Geology and Geophysics* **8**, 680–705.

Matthews, N. E. (2011). Magma chamber assembly and dynamics of a supervolcano: Whakamaru, Taupo Volcanic Zone, New Zealand. Oxford, University of Oxford.

Matthews, N. E., Pyle, D. M., Smith, V. C., Wilson, C. J. N., Huber, C. & van Hinsberg, V. (2012a). Quartz zoning and the pre-eruptive evolution of the ~340-ka Whakamaru magma systems, New Zealand. *Contributions to Mineralogy and Petrology* **163**, 87–107.

Matthews, N. E., Smith, V. C., Costa, A., Durant, A. J., Pyle, D. M. & Pearce, N. J. G. (2012b). Ultra-distal tephra deposits from super-eruptions: Examples from Toba, Indonesia and Taupo Volcanic Zone, New Zealand. *Quaternary International* **258**, 54–79.

Pamukçu, A. S., Carley, T. L., Gualda, G. A. R., Miller, C. F. & Ferguson, C. A. (2013). The evolution of the Peach Spring giant magma body: Evidence from accessory mineral textures and compositions, bulk pumice and glass geochemistry, and rhyolite-MELTS modeling. *Journal of Petrology* **54**, 1109–1148.

Pamukçu, A. S., Gualda, G. A. R., Bégué, F. & Gravley, D. M. (2015a). Melt inclusion shapes: Timekeepers of short-lived giant magma bodies. *Geology* **43**, 947–950.

Pamukçu, A. S., Gualda, G. A. R., Ghiorso, M. S., Miller, C. F. & McCracken, R. G. (2015b). Phase-equilibrium geobarometers for silicic rocks based on rhyolite-MELTS—Part 3: Application to the Peach Spring Tuff (Arizona–California–Nevada, USA). *Contributions to Mineralogy and Petrology* **169**, 1-17.

Pamukçu, A. S., Gualda, G. A. R. & Gravley, D. M. (2021). Rhyolite-MELTS and the storage and extraction of large-volume crystal-poor rhyolitic melts at the Taupō Volcanic Center: a reply to Wilson et al. (2021). *Contributions to Mineralogy and Petrology*. **176**, 1-16.

Pillans, B., Kohn, B. P., Berger, G., Froggatt, P., Duller, G., Alloway, B. & Hesset, P. (1996). Multi-method dating comparison for mid-Pleistocene Rangitawa Tephra, New Zealand. *Quaternary Science Reviews* **15**, 641–653.

Pitcher, B. W., Gualda, G. A. R. & Hasegawa, T. (2021). Repetitive Duality of Rhyolite Compositions, Timescales, and Storage and Extraction Conditions for Pleistocene Caldera-forming Eruptions, Hokkaido, Japan. *Journal of Petrology*. **62**, egaa106.

Reed, S. J. B. & Ware, N. G. (1973). Quantitative electron microprobe analysis using a lithium drifted silicon detector. *X-Ray Spectrometry*. **2**, 69–74.

Reid, M. R. & Vazquez, J. A. (2017). Fitful and protracted magma assembly leading to a giant eruption, Youngest Toba Tuff, Indonesia. *Geochemistry Geophysics Geosystems* **18**, 156–177.

Ritchie, N. W. M., Newbury, D. E. & Davis, J. M. (2012). EDS Measurements of X-Ray Intensity at WDS Precision and Accuracy Using a Silicon Drift Detector. *Microscopy and Microanalysis* **18**, 892–904.

Saunders, K., Morgan, D. J., Baker, J. A. & Wysoczanski, R. J. (2010). The Magmatic Evolution of the Whakamaru Supereruption, New Zealand, Constrained by a Microanalytical Study of Plagioclase and Quartz. *Journal of Petrology* **51**, 2465–2488.

Shamloo, H. I. & Till, C. B. (2019). Decadal transition from quiescence to supereruption: petrologic investigation of the Lava Creek Tuff, Yellowstone Caldera, WY. *Contributions to Mineralogy and Petrology* **174**, 1-18.

Shoji, S., Nanzyo, M. & Dahlgren, R. (1994). *Volcanic Ash Soils: Genesis, Properties and Utilization*. Elsevier: Amsterdam, Netherlands.

Simon, J. I. & Reid, M. R. (2005). The pace of rhyolite differentiation and storage in an “archetypical” silicic magma system, Long Valley, California. *Earth and Planetary Science Letters* **235**, 123–140.

Smithies, S. L., Harmon, L. J., Allen, S. M., Gravley, D. M. & Gualda, G. A. R. (2023). Following magma: The pathway of silicic magmas from extraction to storage during an ignimbrite flare-up, Taupō Volcanic Zone, New Zealand. *Earth and Planetary Science Letters* **607**, 118053.

Stelten, M. E., Cooper, K. M., Vazquez, J. A., Calvert, A. T. & Glessner, J. J. G. (2014). Mechanisms and timescales of generating eruptible rhyolitic magmas at Yellowstone Caldera from Zircon and sanidine geochronology and geochemistry. *Journal of Petrology* **56**, 1607–1642.

Swallow, E. J., Wilson, C. J. N., Myers, M. L., Wallace, P. J., Collins, K. S. & Smith, E. G. C. (2018). Evacuation of multiple magma bodies and the onset of caldera collapse in a supereruption, captured in glass and mineral compositions. *Contributions to Mineralogy and Petrology* **173**, 1–22.

van Achterbergh, E., Ryan, C. G., Jackson, S. E. & Griffin, W. L. (2001). Data reduction software for LAICPMS: appendix. In: Sylvester, P. J. (ed.) *Laser ablation ICPMS in the Earth Sciences: Principles and Applications*. Mineralogy Association Canada Short Course Series, 224–239.

Watson, E. B. & Harrison, T. M. (1983). Zircon saturation revisited: temperature and composition effects in a variety of crustal magma types. *Earth and Planetary Science Letters* **64**, 295–304.

Wilson, C. J. N. & Charlier, B. L. A. (2009). Rapid rates of magma generation at contemporaneous magma systems, taupo volcano, New Zealand: Insights from U-Th model-age spectra in Zircons. *Journal of Petrology* **50**, 875–907.

Wilson, C. J. N. & Charlier, B. L. A. (2016). The life and times of silicic volcanic systems. *Elements* **12**, 103–108.

Wilson, C. J. N., Gravley, D. M., Leonard, G. S. & Rowland, J. V. (2009). Volcanism in the central Taupo Volcanic Zone, New Zealand: tempo styles and controls. In: Thordarson, T., Self, S., Larsen, G., Rowland, S. K. & Hoskuldsson, A. (eds) *Studies in Volcanology: The Legacy of George Walker*. *Special Publications of IAVCEI*, 225–247.

Wilson, C. J. N., Houghton, B. F. & Lloyd, E. F. (1986). Volcanic history and evolution of the Maroa-Taupo area. In: Smith, I. E. M. (ed.) *Late Cenozioc Volcanism in New Zealand*. Wellington: The Royal Society of New Zealand Bulletin **23**, 194–223.

Wilson, C. J. N., Houghton, B. F., McWilliams, M. O., Lanphere, M. A., Weaver, S. D. & Briggs, R. M. (1995). Volcanic and structural evolution of Taupo Volcanic Zone, New Zealand: a review. *Journal of Volcanology and Geothermal Research* **68**, 1–28.

TABLES

1. General descriptions of each tephra unit in the Kohioawa and Ōtarawairere sections
2. Detailed descriptions of the horizons at the Kohioawa and Ōtarawairere sections
3. Distinguishing characteristics of Kohioawa tephra types

APPENDICES

1. The characteristics of the magma types from Brown *et al.* (1998) using whole rock data from pumice clasts
2. Major- and trace-element compositional means and 1-sigma uncertainties of glass data from clasts, including geothermometry and geobarometry modeling results
3. USGS RGM standard major element data

Table 1

Unit	Thickness (KS; OS)	Samples (KS)	Samples (OS)	General Field Characteristics	Magma Type	Mineralogy from field
Tablelands	55 cm; 170 cm	OK220707-1B	OK240707-1A	~3 horizons at both KS and OS; at OS, Tablelands sits atop a graywacke gravel base; layers vary from light cream/pink ash to orange-light brown ash and sand; mostly fine-grained, clay-sand, alternating layers with conspicuous biotite; the top of both sequences is finer grained, firm clay, with more sand at OS; the top of the sequence grades into a soil at OS and grades into soil at an adjacent outcrop at KS	Tablelands+Paerata	plag+qtz+amph+bt
Paerata	150 cm; 205 cm	OK220707-1C; WHAK432A; WHAK432B; OK220707-1E; WHAK432C; OK220707-1F	Ōtarawairere-B	1 continuous horizon with subtle variations in grain size that define internal packages; the top and bottom of the package are fine-coarse clay-silt sized ash dominated; the main package of the unit is yellow-orange, massive with subtle variations in grain size (coarse sand to medium lapilli), grain supported with mostly fine pumice lapilli, lithics, and crystals; there is a conspicuous 20 cm thick black organic soil at the top of the unit that grades into the main package at KS; sharp contact that varies in thickness at OS	Tablelands+Paerata	plag+qtz+opx+amph+bt

Kohioawa	345 cm; 370 cm	OK220707-1G; WHAK432L; OK220707-1I; WHAK432D; WHAK432E; OK220707-1L; WHAK432F; OK220707-1N; WHAK432G; OK220707-1O	OK240707-1C; OK240707-1D; OK240707-1E; OK240707-1F	4 horizons with the thickest ~220 cm thick; at OS, base is grain supported, yellow-rust colored alternating layers of ash to fine pumice lapilli; at KS, two basal units are massive, grain supported ash-sand and cream-light brown fine-coarse ash on top; subtle crossbeds mark the beginning of the thickest horizon; thickest horizon is yellow, massive, and has fluctuations in grain size that define internal, grain supported packages of varying sized sand-pumice lapilli; sharp contact with the upper horizons; top package is defined by thin alternating coarse and fine grain supported ash layers with a light brown clay; firm clay (paleosol at KS) at the top	Kohioawa type A; Kohioawa type B; Kohioawa type C	plag+qtz+amph+opx+bt
Murupara-Bonisch	180 cm; 350 cm	OK220707-1P; OK220707-1Q; WHAK432H; WHAK432I; WHAK432J	OK240707-1J; OK240707-1L	at KS, ~8 thinner horizons, predominantly grain supported, cream to yellow to light brown, fine pumice lapilli to silt-sized ashy alternating horizons, generally ~5-10 cm thick; several horizons fine upward; at OS, fewer defined horizons with thicker, fine-grained clay-silt; wavy bedding and alternating layers between thicker, finer grained layers; a soild separates the upper horizons at both locations; at KS, accessed with a ladder to the left of the main outcrop; upper layers are ashy and less consolidated below a friable sandy deposit and below the Matahina ignimbrite	Murupara-Bonisch type A; Murupara-Bonisch type B	qtz+plag+amph+opx

Table 2

Kohioawa Section

Starting cm	Ending cm	Thickness	Mineralogy (in field)	Horizon Description	Samples	Location of Sample	Unit	Mineral Componentry
-1	9	10	plag + qtz + amph + bt	Unit grades into sand below, contact is distinct but not sharp			Tablelands-C	
9	22	13		pink to cream colored mottling/layers, very fine ash that grades into fine to coarse ash that is light gray; paleosol at adjacent outcrop at the top of this layer			Tablelands-C	
22	40	18	qtz + plag + bt + amph	light gray alternations between fine grain supported layers (medium to coarse sand size) and fine to coarse ash layers, conspicuous biotite	OK220707-1B	35	Tablelands-D	plag + qtz + cum? + hbl + opx + ox
40	53	13		creamy white very fine ash; paleosol at adjacent outcrop			Tablelands-D	
53	59	6		base is 6cm with fine to coarse ash layers alternating with grain supported sand-sized layers; fine ash is light gray in color, biotite bearing.			Paerata	
59	184	125	WHAK432A – qtz + amph + opx; WHAK432B – plag + qtz + opx + amph; OK220707-1E – plag + qtz + opx + amph; OK220707-1F plag + qtz + opx + amph	yellowish to orange colored, massive with subtle variations in grain sizes that define internal packages. The top and bottom of the unit contain find and coarse ash, but the main body is grain supported with a range of pumice lapilli sizes (mostly fine), lithics, and crystals. there is conspicuous biotite towards the base of the unit	OK220707-1C; WHAK432A; WHAK432D, OK220707-1D; OK220707-1E; WHAK432C; OK220707-1F	70; 75; 100 (45 cm above base of unit); 125 (65 cm above base of unit); 140; 175 (top of coarse-grained section)	Paerata	OK220707-1C – plag + qtz + cum? + hbl + opx + ox; OK220707-1E – plag + qtz + cum? + hbl + opx + ox
184	204	20		black organic top grading into medium then lighter brown very firm clay (paleosol). This grades into the top of the unit below. Conspicuous woody fragments			Paerata	

204	226	22	plag + qtz + amph + opx + bt	massive, grain supported fine pumice lapilli, lithic, crystal unit. Yellow to rust colored	OK220707-1G	215	Kohioawa	plag + qtz + opx + hbl + ox
226	236	10		cream to light brown fine to coarse ash with scattered crystals and some obsidian lithic; normally graded with a very thin pink strip near the base			Kohioawa	
236	261	25	plag + qtz + amph + opx + bt	cross-bedded with lensoid shaped layers of better sorted grains (reworked base) Pervasive rust colored iron oxide staining	OK220707-1H		Kohioawa	
261	481	220	plag + qtz + amph + opx + bt	sharp upper contact but no sign of erosion or reworking (little to no time break). Massive yellowish unit with vertical fluctuations in pumice lapilli size and concentration that define a subtle bedding. Grain supported, generally crystal rich with >1% lava lithics. From OK220707-1I through OK220707-1O, crystal rich matrix for the entire unit. There are crystal poor and crystal rich pumice clasts.	OK220707-1I; WHAK432D; OK220707-1J; WHAK432E; OK220707-1K; OK220707-1L; OK20707-1M, WHAK432F; OK220707-1N	265; 287; 305; 333; 355; 380; 422; 465	Kohioawa	OK220707-1I – plag + qtz + opx + hbl + ox ±bt; OK220707-1L – plag + qtz + opx + bt + hbl + ox
481	547	66	plag + qtz + bt + amph	light brown, very firm clay with developed but thick paleosol that grades down (by color) into yellowish, not as firm to fine to coarse ash with conspicuous biotite. Lower 48 cm is alternating fine to coarse ash layers and grain supported very fine pumice lapilli lithics and crystals. Log does not represent the fine scale detail of those alternations. Biotite is consistent throughout.	WHAK432G; OK220707-1O	490; 512	Kohioawa	OK220707-1O – plag + qtz + bt + hbl + opx + ox
547	552	5	plag + qtz + amph + opx	yellowish, grain supported massive fine pumice lapilli, lithics, crystals (although less crystals and <1% lithics compared with units above)	OK220707-1P	550	Murupara-Bonisch	plag + qtz + hbl + opx + ox ±bt
552	565	13		variable thickness because of the wavy top, white to cream fine ash. Has same soft-sediment deformation as fine ash layers seen elsewhere, i.e., Rangitawa tephra in Awatarariki Stream			Murupara-Bonisch	

565	572	7		yellow color, variably graded, grain supported fine pumice lapilli, lithics, crystals. Undulating basal contact with micro valley fill-like structures.			Murupara-Bonisch	
572	577	5		cream to light brown fine ash with scattered fine pumice lapilli, lithics, and crystals			Murupara-Bonisch	
577	590	13	qtz + plag + amph + opx	cream to light brown silty ash with some fine pumice lapilli on top of variably graded clast supported pumice lapilli and lithic, crystal, massive, yellowish color, >5% lithics of obsidian, pumice up to 10mm	OK220707-1Q	585	Murupara-Bonisch	plag + qtz + hbl + opx + ox
590	615	25		light brown fine silt (weak paleosol maybe) on top of mostly clast supported fine pumice lapilli, crystals, and ash, normal to reverse graded, >5% lava lithics, qtz, and amphibole. Unit is yellowish in color and massive, well sorted	OK220707-1R		Murupara-Bonisch	
615	725	110		alternating fine (up to 3 cm) layers of coarse ash to fine lapilli layers and finer ash layers that are different shades of white. WHAK432H is at 670 cm in a fine lapilli layer. WHAK432I is a fine lapilli layer at 720 cm and just below contact with grayish white fine ash. WHAK432J is base of grayish white fine ash that is >1 m thick. Looking along strike where it is exposed in cliff. This is below a friable sand deposit (beach?) below the Matahina ign.	WHAK432H; WHAK432I; WHAK432J	670; 720; 730	Murupara-Bonisch	
Total Thickness		**726**						

Ōtarawairere Section

Starting cm	**Ending cm**	**Stated thickness**		**Horizon Description**	**Samples**	**Location of Sample**	**Unit**	**Mineral Componentry**
-10	0	10		graywacke gravel base			Basement	
0	27	27		medium brown clay with scattered graywacke pebbles	OK240707-1A	5	Tablelands-B	plag + qtz + bt + hbl + ox

27	77	50	alternating coarse sand-sized and fine-ash layers, gray color except for the bottom 10 cm. Log does not accurately depict layers. Conspicuous qtz and biotite throughout this unit			Tablelands-C	
77	124	47	light orangish brown very firm clay with crystals including biotite. Grades into biotite bearing material below. This looks like a loess paleosol			Tablelands-C	
124	133	9	orange, not as firm, more sand than clay, closer to grain supported than material below and above, ferro-mag crystal poor (tephra?) gradational contacts			Tablelands-D	
133	160	27	light brown to orange clay to fine sand, firm not as much clay as 47 cm thick unit below, biotite bearing (loess paleosol?)			Tablelands-D	
160	325	165	normally graded lower 10 cm that is rust stained at base and grades up into a light gray color, crystal-rich qtz, bt, and amph. Sharp change in grain size at this point (10 cm above base of unit), no biotite, possible cummingtonite. 165 cm thick massive, yellow colored, poorly sorted with very little variation in pumice concentrations (i.e., no real obvious or subtle bedding), grain supported, predominantly pumice ranging from sane size up to ~10 mm. lithic poor, crystal rich with large qtz, feldspar, opx, amph	Unit-B Ōtarawairere	190 and 310 mixed	Paerata	plag + qtz + cum? + hbl + opx + ox
325	364	39	light brown to orange clay dominant with scattered crystals, firm (loess paleosol), grades into the unit below and has a sharp irregular contact on top. Thickness varies laterally (up to 60 cm thick in places)			Paerata	
364	416	52	Orange to yellow massive, reverse to normal graded grain supported irregular but sharp upper contact which means the thickness varies	OK240707-1C	415	Kohioawa	

			considerably (< 30 cm in places), crystal rich with plag qtz opx, amph				
416	431	15	light brown, thin alternating layers of ash matrix, fine pumice lapilli, obsidian lithics, and crystals of grain supported crystal rich layers; qtz, plag and large opx crystals			Kohioawa	
431	456	25	low angle cross beds, reworked base of plinian0style fall, yellow to rust colored			Kohioawa	
456	626	170	yellow to rusty orange, massive to subtle pumice cementation bedded with noticeable sub packages of finer and coarser grainsizes. Grain supported, Plinian style. Crystal rich with conspicuous quartz and biotite. Did not record mineralogy at different levels here like at Kohioawa section; (higher up notes) This marks the approximate height where Darren noted the top of this unit at the Kohioawa cliff section; It was a more obvious contact there where it went from a massive Plinian style deposit to a well bedded and layered sequence. Here, it is a more gradational relationship. From this point to the base is 170 cm. (see sharp color contrast, orange to light gray, to mark this height in photos 53-57).	OK240707-1D	610	Kohioawa	
626	678	52	plane-parallel bedded coarser grained supported beds and fine to coarse ash beds. Most of these layers contain biotite. Log is not an accurate depiction.	OK240707-1E; OK240707-1F	660; 675	Kohioawa	OK240707-1E – plag + qtz + bt>>hbl + opx? + ox
678	735	57	light gray very fine ash with conspicuous crystal rich and coarse pumice sand layers. Biotite throughout			Kohioawa	
735	780	45	sequence of plan parallel to wavy bedded coarse and fine-grained layers. The wavy bedding looks more like contorted deformation due to loading above as opposed to primary low angle			Murupara-Bonisch	

			crossbedding. Most layers have obvious biotite and amphibole.			
780	871	91	light gray ash with a ~2 cm thick weakly developed paleosol on top (not sure this is a paleosol). The ash is very fine grained but does not contain paleosol-like clay, crystal poor with some biotite and amphibole. The weakly developed paleosol on top is purplish brown and firm due to clay content. Can still see glass in the body of this unit underneath a hand lens.			Murupara-Bonisch
871	1085	214	(~15 cm) scattered angular pumice up to 5-7 cm fragments and relatively crystal rich with conspicuous amphibole and biotite. Very poorly sorted with ash matrix (can see glass shards under hand lens). (115 cm) scattered angular pumice lapilli (up to 10 mm) and lithics with moderate crystal content (not as rich as base). Largest lithics are comparable size to largest pumice. (145 cm) very little pumice, similar crystal content. (top) light gray, massive, very poorly sorted ash with variable amounts of pumice, lithics, and crystals. Top 60-70 cm is very crystal rich with obvious amphibole and biotite. Sorting characteristics, glass shards, similar max pumice and lithic sizes suggests this is an ignimbrite. A firm buff paleosol-loess on top of this unit may be the lateral equivalent of the paleosol between biotite-bearing and non-biotite-bearing ash and crystal layers at Kohioawa fully in cliffs west of Matata. Also recorded an obsidian lithic bearing unit above this which also correlates with beds above same paleosol at Kohioawa	OK240707-1J; OK240707-1L	980; 1080	Murupara-Bonisch
Total Thickness		**1095**				

Table 3

	Kohioawa type A	Kohioawa type B	Kohioawa type C
SiO_2	76.9-77.8	77.2-77.7	77.2-78.1
CaO	0.76-1.07	0.54-0.62	0.47-0.59
TiO_2	0.11-0.21	0.04-0.10	0.03-0.08
FeO	0.97-1.74	0.81-1.09	0.68-1.11
MgO	0.06-0.33	0.01-0.07	0.02-0.11
Sr	43.0-75.6	20.5-25.5	8.03-20.3
Ba	649.-910.	298.-869.	69.1-222.
Mn	222.-365.	383.-424.	378.-492.
Eu	0.30-0.57	0.18-0.59	0.12-0.33
U	2.86-5.99	3.96-4.57	4.19-5.88
Pb	13.7-19.6	14.2-17.6	15.7-21.9
Cs	5.59-8.32	8.16-9.33	8.24-12.3
Zr	74.5-136.	64.4-108.	63.8-98.0
Yb	1.85-2.78	2.58-2.96	2.61-3.58
Y	15.1-23.6	19.0-26.0	21.7-30.3